SHEAR DEFORMATION IN THIN POLYMER FILMS AS A PROBE OF ENTANGLEMENT IN CONFINED SYSTEMS

SHEAR DEFORMATION IN THIN POLYMER FILMS AS A PROBE OF ENTANGLEMENT IN CONFINEED SYSTEMS

By

LUN SI, M. Sc

A Thesis

Submitted to the school of Graduate Studies

In Partial Fulfillment of the Requirements

for the Degree

Master of Applied Science

McMaster University

MASTER OF APPLIED SCIENCE (2003) McMaster University
(Materials Science and Engineering) Hamilton, Ontario

TITLE: Shear Deformation Zone in Thin Polymer Films

as a Probe of Entanglement in Confined Systems

AUTHOR: Lun Si, M. Sc.

SUPERVISOR: Dr. Kari Dalnoki-Veress

NUMBER OF PAGES: X, 71

Abstract

We present the results of our study of the shear deformation zone in free-standing thin polymer films as a probe of entanglement in confined systems. A stretching system was used to uniaxially strain thin polystyrene (PS) films. Atomic force microscopy was used to measure the thicknesses of the shear deformation zone (SDZ), h_c, and the film thicknesses h. The maximum extension ratio $\lambda = h/h_c$, was measured as a function of film thickness. The results show that λ increases with the decreasing film thickness which implies an increase in the entanglement molecular weight in confinement. The same experiments were carried out for thin PS film with different molecular weights. A tentative model was developed to explain the experimental results and found to be in good agreement with the data. More exciting is the fact that the model predicts a scaling dependence on the polymer molecular weight which was also observed.

Acknowledgements

I would like to express my gratitude to my supervisor, Dr. Kari Dalnoki-Veress from the bottom of my heart. I really appreciate his invaluable guidance and advice throughout the period of my candidature in the Department of Materials Science & Engineering, McMaster University. Especially I will never forget the period when I was doing my thesis. He helped me go through the most difficult time of these two years. I have really learned a lot from him. That will be with me all my life.

I would also thank Mike for his large amount of help. He always helped me overcome some difficulties and solve some problems whatever in research or in daily life. My appreciation is also extended to other colleagues including Adam, Andrew, Marie-Josee, Andrea and John. Their friendship and help during my study will always be a wonderful memory in my mind.

Words cannot express the debt of thanks I owe to my parents and my wife. Without their encouragement and support I would not have had the strength to finish this project.

And last but not least, I would like to acknowledge the support of McMaster University for granting me a scholarship.

Table of Contents

List of Figures:

List of Tables:

Chapter 1 Introduction

1.1 A brief introduction to polymers

Polymers are a subclass of macromolecules which consist of long chains of molecular units or '*monomers*' which are connected together by covalent bonds. The word "polymer" originally comes from the Greek words 'poly'-'mer' which means many-part. The process by which monomers are joined to form a polymer is known as polymerization. Polymers can range from short chains with molecular weight, $M_w \sim 5000$ g/mol, to very long chains with $M_w \sim 10^7$ g/mol [1].

The use of polymeric materials in industry and technology is increasing year-by-year and in many applications polymers are replacing conventional materials such as metals, wood as well as natural fibers such as cotton and wool. Polymers are also common in nature as DNA, RNA, proteins and polysaccharides, which clearly play important roles in plant and animal life.

1.1.1 Homopolymers and copolymers

The diversity of polymers is overwhelming. There are many polymers with linear and non-linear structures which are shown in Figure 1.1. For example, non-linear polymers can be branched, star, network and ladder polymers. A polymer derived from

one species of monomer, is called a *homopolymer*. The structure of a polymer can be represented by that of the repeat unit enclosed by brackets. Thus the homopolymer

–A-A-A-A-A-A–

is represented by $[A]_n$ where n is the number of repeat units linked together to form the macromolecule.

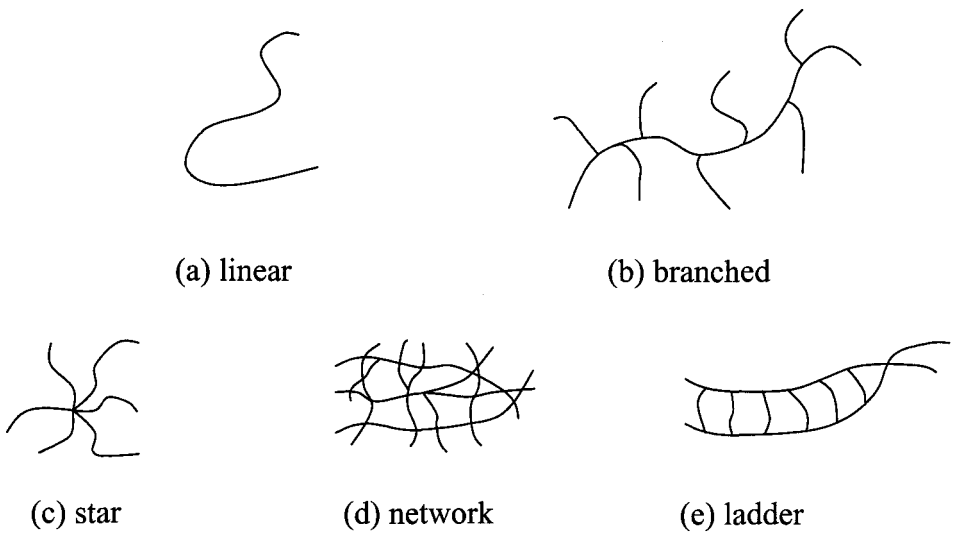

Figure 1.1 Different polymer architectures for homopolymers: (a) linear, (b) branched, (c) star, (d) network, (e) ladder.

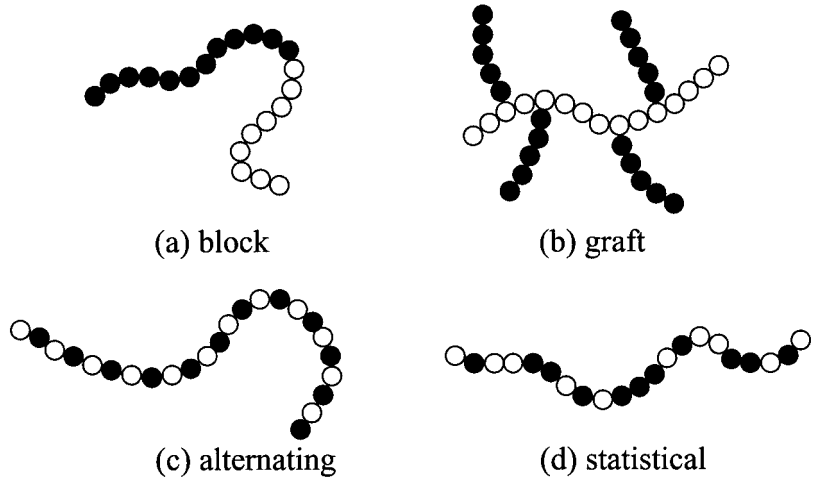

Figure 1.2 Example of a few of the different polymer architectures for copolymers: (a) block, (b) graft, (c) alternating, (d) statistical.

A copolymer is a polymer derived from more than one species of monomer. There are several categories of copolymers, each being characterized by a particular form of arrangement of the repeat units along the polymer chain as shown in Figure 1.2. There are a lot of potential applications for copolymers. Some copolymers can be used for biomedical, pharmaceutical and food applications. For instance, some block copolymers can be used as drug carriers. Due to their typical physical properties for wetting and detergency, some copolymer can be use as detergent. Some copolymers have some potential applications in nano-technology as well [1].

1.1.2 Molecular weight and degree of polymerization

Many properties of polymers show a strong dependence on the size of the polymer chains, so it is very important to characterize their dimensions. During the polymerization

process, smaller molecules are synthesized into large macromolecules. However, not all polymer chains will grow to exactly the same length, resulting in a distribution of chain lengths or molecular weights.

There are several ways of defining average molecular weight. *The number average molecular weight* M_n is obtained by the total mass of the system divided by the number of molecules. If n_i is the number of chains with mass M_i and the weight of all the chains with length N_i in our ensemble is $w_i = n_i M_i$. We can write

$$\overline{M}_n = \frac{\sum n_i M_i}{\sum n_i} = \frac{\sum w_i}{\sum (w_i / M_i)}.$$

Another way to define average molecular weight is as the *weight average molecular weight* which is given by

$$\overline{M}_w = \frac{\sum w_i M_i}{\sum w_i} = \frac{\sum n_i M_i^2}{\sum n_i M_i}.$$

The average chain size of a polymer can also be expressed as the *degree of polymerization n*, which represents the average number of monomer units in a chain. As before, we can define both the number-average (n_n) and the weight-average (n_w) degrees of polymerization as

$$n_n = \frac{\overline{M}_n}{m}, \text{ and } n_w = \frac{\overline{M}_w}{m};$$

where m is the monomer molecular weight. The *polydispersity index* is a measure of the distribution of molecular weight in a sample. In polymers, the polydispersity index (PI) is given by the ratio of M_w and M_n [2]. A monodisperse sample has PI = 1, while a realistic monodosperse sample had PI ~ 1.1.

1.2 Chain conformation in polymers

Polymer chains are flexible. For example, we can have rotations of the strong covalent C-C bond in the backbone. As a result there is some mobility. In figure 1.3, we show a standard example of how a rotation about the backbone can result in a flexible chain. In the example, as long as we keep the bond angle θ fixed, the third atom is free to move. Successive random rotations about the backbone as shown in figure 1.3a, will result in a random chain conformation as depicted in Figure 1.3b [2].

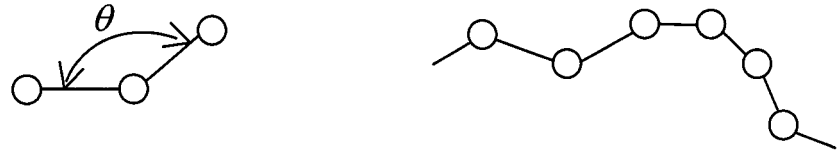

(a) (b)

Figure 1.3 Schematic representations of how polymer chain shape is influenced by the positioning of backbone carbon atoms. (a) the angle between neighboring bonds is fixed; (b) the twisted chain segment.

For polymers in the melt state, the conformation of the chains can be shown to be that of a three dimensional random walk (i.e. Brownian motion) as shown in Figure 1.4.[2] Because a 3-D random walk is an open structure, many chains interact with each other in order to build up the required density.

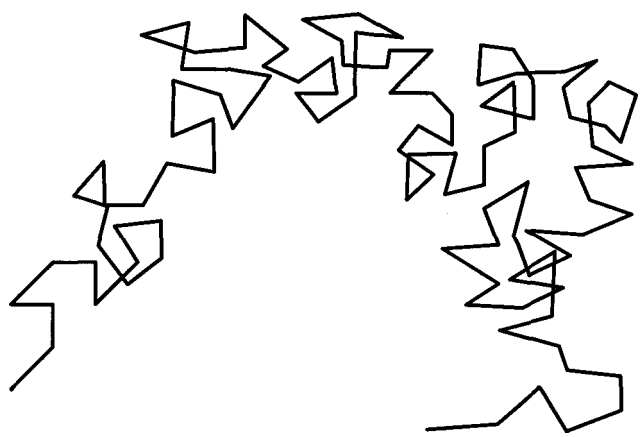

Figure 1.4 Representation of a single polymer chain molecule as a random walk.

1.3 Length scales of polymer chain

In the present work, we will be discussing entanglements in thin polymer films. In order to understand entanglements, we first need to develop a way to describe the size of polymer molecules. There are many different length scales related to polymer molecules ranging from the monomer length to the length of a fully extended chain. For our

purposes, two related measures of polymer chains are most physically relevant: (a) the average end-to-end distance (R_{ee}); and (b), the radius of gyration (R_g).

1.3.1 End-to-end distance R_{ee}

The root-mean-square end-to-end distance R_{ee} is defined by the following equation:

$$R_{ee} = \left\langle \vec{R}_{ee}^{\,2} \right\rangle^{1/2}$$

where $\vec{R}_{ee}$ is a vector which points from the center-of-mass of the first monomer to the center-of-mass of the last monomer [3]. (Figure 1.5)

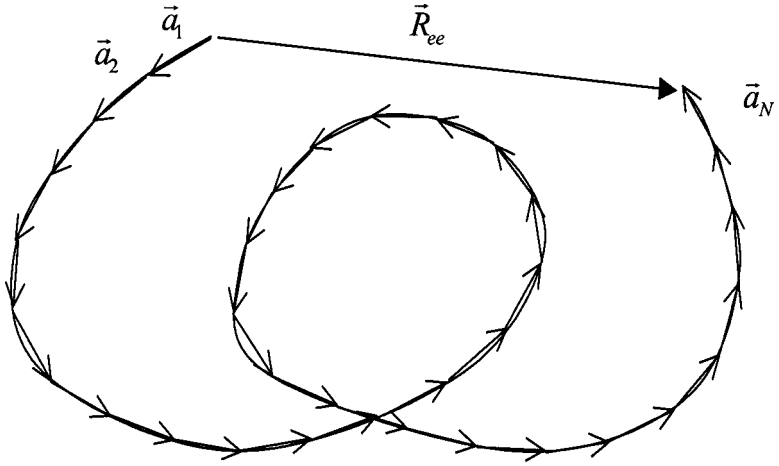

Figure 1.5 Schematic polymer chain as a series of vectors with length a.

Polymers are long chain molecules and are flexible at some length. While there is some orientational correlation between neighboring segments on the chain, we can define the persistence length as related to the length beyond which segments have lost this orientational order:

$$l_p = l_0 \exp(E/kT);$$

where E is the barrier to rotation of bonds, l_0 is a few Angstroms, k is the Boltzman constant and T is temperature. Hence, l_p describes the minimum step size for which random walk statistics are valid. Since there is no correlation between neighbouring segments when they are defined as segments greater than the persistence length, the contour of the entire chain can be represented by a series of steps in random directions.

In order to calculate R_{ee}, we first need to look at an interesting self-similarity that applies to long chains. In this description we have assumed that there is no interaction between widely separated segments along the chain, and while the segments i, i+1, and i+2 might be correlated, i and i+100 are not correlated.

In this rescaled description, the polymer consists of many rigid rods (or segments) of the same length a. Vector $\vec{a}_i$ represents the ith segment where $a > l_p$ (see Figure 1.5). Here we take the number of segments to be given by N with $1 \leq i \leq N$; and in general, there are many vectors $\vec{a}_i$ with different segment lengths which can form the end-to-end vector

$$\vec{R}_{ee} = \sum_{i=1}^{N} \vec{a}\,.$$

As a result, the chain can be described by different combinations of a and N.

This self-similarity is valid for a range of a values as long as a is greater than the persistence length. Clearly, there is some length l for which when $a > l$

$\langle \vec{a}_i \cdot \vec{a}_{i+1} \rangle = 0$.

For this choice of a, the chain consists of individual segments that are freely-jointed and this chain conformation is equivalent to a random walk. Each description (N, a) of the chain is self-similar. There is obviously a maximum limit for a, since then the segment length becomes comparable to $\vec{R}_{ee}$. This model is only valid for *'ideal'* chains, which exhibit no interaction, on average, between segments that are widely separated. The *'ideal'* case is found to be valid for chains in the melt, since each segment is surrounded by many other chains. In the melt, long range interactions are screened, i.e. there is no difference between the interaction of two segments on the same chain and the interaction of two segments on different chains. Isolated chains are typically not ideal because the solvent does not screen the interaction between different parts of the same chain. However this is not the case for *'θ-solvents'* in which the screening is perfect and the chains can be assumed to be ideal.

For ideal chains, represented by a random walk, it is straight forward to calculate the root-mean-square end-to-end distance as follows:

$R_{ee}^2 = \langle \vec{R}_{ee}^2 \rangle$

$$= \langle (\vec{a}_1 + \vec{a}_2 + \vec{a}_3 + ...) \cdot (\vec{a}_1 + \vec{a}_2 + \vec{a}_3 + ...) \rangle$$

$$= \langle \vec{a}_1 \cdot \vec{a}_1 \rangle + \langle \vec{a}_2 \cdot \vec{a}_2 \rangle + \langle \vec{a}_3 \cdot \vec{a}_3 \rangle + ... \langle \vec{a}_N \cdot \vec{a}_N \rangle$$

$$+ \langle \vec{a}_1 \cdot \vec{a}_2 \rangle + \langle \vec{a}_1 \cdot \vec{a}_3 \rangle + \langle \vec{a}_2 \cdot \vec{a}_1 \rangle + \langle \vec{a}_3 \cdot \vec{a}_1 \rangle + ...$$

Because on average there is no interaction between different segments for a random walk, the sum of all the cross terms in the equation above vanishes. We have

$$R_{ee}^2 = \langle \vec{a}_1 \cdot \vec{a}_1 \rangle + \langle \vec{a}_2 \cdot \vec{a}_2 \rangle + \langle \vec{a}_3 \cdot \vec{a}_3 \rangle + ... \langle \vec{a}_N \cdot \vec{a}_N \rangle = Na^2 .$$

The end-to-end distance is a very important length scale for this project as it describes the size of a polymer chain and the volume pervaded by a chain [3]. Practically, one obtains the value of R_{ee} for polymer melts by using the ratio of R_{ee}^2 / M_w that has been tabulated for chains in θ-solvent conditions. For example, for polystyrene, the size of the polymer chain can be calculated from the molecular weight by using $R_{ee}^2 / M_w = 5.4 \times 10^{-3}$ (nm^2 mol g^{-1}).

1.3.2 The radius of gyration R_g

An alternative measure of the size of a polymer chain is provided by its radius of gyration, which may be measured by light scattering experiments. The radius of gyration R_g is defined as average root-mean-squared distance of all the repeating units of the chain from the center of mass of the chain

$$R_g = \frac{1}{Nm}\left\langle \sum_{i=1}^{N} m\vec{s}_i \cdot \vec{s}_i \right\rangle;$$

where m is the mass of a segment and the vector $\vec{S}_i$ points from the center of mass of the molecule to the center of segment i. R_g has a similar scaling dependence on the molecular weight as R_{ee}. For a long chain, it is possible to show that

$$R_g = a\sqrt{\frac{N}{6}};$$

and then the ratio of R_g to R_{ee} is given by

$$\frac{R_g}{R_{ee}} = \frac{a\sqrt{N/6}}{a\sqrt{N}} = \sqrt{\frac{1}{6}} \approx 0.41.$$

1.4 The glass transition temperature

The glass transition is an important phenomenon for polymers because many properties are strongly affected through the transition. Most importantly, a polymer is a viscous liquid above the glass transition temperature, while it is an amorphous solid (frozen liquid like state) below the transition. The glassy state can be thought of as a form of matter, which has physical properties similar to a crystalline solid but has the molecular order of a liquid [4].

1.5 Entanglements of polymers

Entanglements of polymer chains are important for discussing deformations of polymers because they have an important effect on the mobility of the molecules. When we deform the glassy polymer, some entanglements (knots in the network) between segments of polymer chains will remain intact and act like effective cross-links in the system. Entanglements strongly affect dynamic properties of polymer melts such as viscosity and diffusion and are responsible for the elastic behaviour in the visco-elastic melt on short time scales. Entanglements can also affect some high strain properties such as the natural draw ratio, craze extension ratio, and toughness. An important parameter is the entanglement molecular weight which is described by the *average* molecular weight between entanglements along a chain M_e. The entanglement molecular weight can be determined from measurements of the shear modulus of the melt in the rubbery plateau region just above the glass transition temperature T_g [4]. The entanglement density (which is inversely proportional to the entanglement molecular weight and corresponds to the number of entanglements per unit volume) is important for describing mechanical properties like crazing and shear deformation which will be discussed in the next sections.

1.6 What is a craze?

Crazing is a common phenomenon in our daily life. For example, if we bend a piece of glassy polymer (like a transparent pen), there are often some white lines appearing within the polymer. These white lines are the crazes and appear white because of light

that is scattered off these structures. Crazes in glassy polymers are crack-like defects although they differ significantly from a crack. With the high magnification of electron microscopy, it is found that crazes are not true cracks, but consist of an interconnected network of voids bridged by small fibrils of polymer. Crazing can be though of as the formation of a narrow fibrillated region surrounded by deformed material in the strained glassy polymers. This property of crazes is important because it is responsible for brittle failure in glassy polymers [5]. Now we discuss how crazes form during the straining process. If a tensile load is applied to a glassy polymer, initially some interconnected micro-voids will form, which grow into a fully developed matrix of voids and thin fibrils. As shown in figure 1.6a, the two craze interfaces are bridged by tiny fibrils. Electron microscopy has shown that these fibrils have dimensions with a diameter of 5-30 nm [11]. If the load is increased further, these fibrils will elongate and break. In the final stage, these micro-voids grow and coalesce to form a full crack (Figure 1.6b). Crazes are the precursors to full cracks which lead to brittle fracture in glassy polymers.

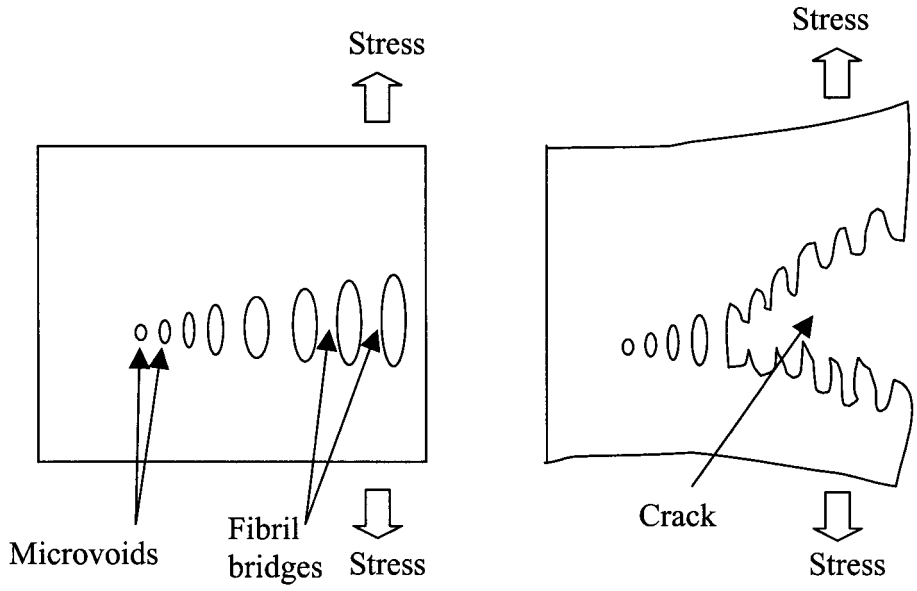

Figure 1.6 Crazing process (a) the formation of microvoids and filbrils; (b) the formation of a crack.

1.7 What is a deformation zone?

Some glassy polymers deform by a shear deformation without forming the fibril/void structure of the craze [8-10]. This kind of deformation can be found to occur during tensile deformation of thin sheets as plane stress shear deformation zones (SDZ) [11,12]. The surface of these zones are found to be uniform and the structure of fibrils and voids is not observed in this mode of failure.

By changing various parameters (temperature, strain rate, architecture, blend composition, and entanglement network), the polymer can have a transition from crazing to shear deformation when a strain is applied.

1.8 Crazing process

Normally there are three steps for the formation of a craze: (1) craze nucleation; (2) craze growth; (3) craze break down. These three steps are discussed in turn below. Detailed discussion can be found in the excellent review by Kramer and Berger [16].

1.8.1 Craze nucleation

In the early study of crazing, Argon and co-workers reported [13] that there is a time delay between the application of stress and the appearance of crazes. This is thought to be the result of a barrier which prevents the nucleation of a craze. Crazes are usually observed to nucleate on the surface of the sample beneath defects such as surface grooves, steps or dust particles [13].

1.8.2 Craze growth

There are two mechanisms for craze growth: craze-tip advance and craze thickening.

(1) Craze-tip advance

Normally, just ahead of the craze there is a small zone which is 5-10 nm in size. One explanation for this is the Saffman-Taylor meniscus instability [14]. This instability is

observed in the following case. Suppose there are two flat plates which sandwich a liquid layer. If a force is applied to take the two plates apart, this meniscus instability will be observed at the advancing tip. When a craze moves forwards, there is a wedge-shaped zone of deformed polymer formed just ahead of the craze tip. The deformed polymer is a liquid like due to the high stress and serves as the "fluid" layer, and the undeformed polymer outside this zone serves as the rigid "plate". It is thought that the initial wavelength of the Saffman-Taylor meniscus instability is correlated to the fibril wavelength.

(2) Craze thickening

When a craze grows in area by advancing the craze tip, the craze also increases in the direction normal to the craze surfaces. There are two different mechanisms for craze thickening. One mechanism was suggested by Morgan *et al.* [15]. These authors suggested that once fibrils are formed at the craze, there will be no new polymer drawn into the fibrils at the craze surfaces. The second mechanism was suggested by Lauterwasser and Kramer [5], who suggested that new polymer could be drawn into the fibrils from the craze interfaces. If the applied stress is constant, the craze interfaces would keep the extension ratio of the fibrils constant. This property is called the surface drawing mechanism. This surface drawing mechanism is similar to the cold drawing of macroscopic polymer fibers. This kind of drawing takes place normally by forming a neck with a certain draw ratio. The neck will extend by drawing new polymer into the neck continuously. Therefore, the growth of the neck will not make the polymer weaker because the neck remains load bearing.

1.8.3 Craze fibril breakdown

The growth of the crazes is only the start of the fracture in a glassy polymer. Crazes will grow both in width and in depth until the sample breaks down to form a large void. Clearly, craze growth is a necessary condition for fracture but not a sufficient condition. The controlling step in the fracture for most glassy polymer crazes is the initiation of the first large void, this process is termed craze fibril breakdown [16]. The effect of entanglement density on crazes will be introduced in detail in the next section.

1.9 Review of molecular entanglement for polymers

In this section, a brief review of molecular entanglement will be given.

1.9.1 Effects of entanglement on crazing and shear deformation behavior

Previous experimental results [17-20] of crazes and shear deformation zones in thin polymer films show that the entanglement network of the polymer is very important to study crazes and shear deformation zones. Kramer and co-workers suggested a simplified model which has a density of network chains ν between localized points of entanglement [21]. The entanglement density is given by

$$\nu = \rho N_A / M_e$$

where ρ is the density of the polymer, N_A is Avogadro's number, and M_e is the entanglement molecular weight which has been briefly introduced in Section 1.5 of this chapter.

From extensive experimental studies by Donald and Kramer, it was found that the entanglement density v for thin films of a series of homopolymers, copolymers and polymer blends ranged from 10^{25} m^{-3} to 30×10^{25} m^{-3}. It was found by these authors that the crazing and shear deformation behavior depended on entanglement density v. If the entanglement density of a polymer $v < 4\times10^{25}$ m^{-3}, then there will be only crazing observed for this polymer. If the entanglement density of a polymer in the range of $4\times10^{25} < v < 8\times10^{25}$ m^{-3}, there will be both crazes and SDZ's. If the entanglement density of a polymer $v > 8\times10^{25}$ m^{-3}, only SDZ's are observed [21].

1.9.2 Entanglements at polymer surfaces and interfaces

As mentioned above, crazing and SDZ's are strongly influenced by entanglement density within high molecular weight material. Specifically, it is the entanglements that control the high molecular weight toughness.

Entanglement for bulk polymers is well studied and understood. It was suggested by Fetters *et al.* that the entanglement density is strongly related to the chain topology and hence the packing of the polymer chains determines the entanglements or entanglement molecular weight M_e [22]. These researchers also proposed that the volume pervaded by

a chain is about 10 times the hard-core volume occupied by that chain [22, 23]. If a chain is packed more densely, a higher M_e is required in order to interact with other chains. Conversely, if the chain is extended, a much shorter M_e is required in order to interact with other chains.

Compared with entanglement in the bulk, entanglements near or at interfaces is much less well understood. Recently, Brown, Russell, and co-workers suggested that entanglement might be different close to an interface because the chain packing is perturbed in this region [24,26]. Silberberg proposed a model to describe the chain packing close to an interface [27]. His simulation results showed that the polymer chain configurations close to the interface are different from the bulk configuration as a result of a reflection of chains at an interface. According to this model, the chains at an interface are packed more densely than in the bulk and the entanglement density will be decreased and entanglement molecular weight M_e will be increased. Brown *et al.* [26] also used self-consistent mean-field techniques to obtain the local average chain packing and successfully calculated the entanglement density close to an interface. They also found that for polystyrene chains with M_w = 1,248,000, at about 10 nm from the interface the packing started to be different and the entanglement density was decreased by about an order of 2 close to interface [26]. Other authors have used different calculation approaches to calculate entanglement density with similar results [28].

1.10 Motivation of the project

As discussed above, the entanglements of polymer chains are very important because they strongly influence the dynamical properties of polymer melts such as viscosity and diffusion.

Many groups have shown that there are significant anomalies for two-dimensional thin films (for a recent review see [29] and [30]). Some of the anomalous properties in thin films may be related to the entanglement density near the interface. This is the main reason for the focus of the work presented in this thesis.

Chapter 2 Experimental methods

2.1 Sample Preparation

Sample preparation is very important in this project because the quality of the sample strongly affects deformation behavior of thin polymer film. In this section, detailed methods and procedures will be given.

2.1.1 Spincoating

Spincoating is a common method for the preparation of thin polymer films. Polymer, dissolved in a solvent, is typically dropped onto a spinning substrate. With this technique, it is easy to produce various polymer films with a wide range of film thicknesses by using different concentrations of the solution and the spinning speed of the substrate.

Films can be produced either by dropping solution onto a spinning substrate ('spin-then-drop'), or by first dropping solution onto a stationary substrate and then spinning ('drop-then-spin'). When spincoating, both 'spin-then-drop' and 'drop-then-spin' methods can produce films with similar thicknesses, however some experimentation is often required to determine which of these two approaches results in the most uniform films.

The substrate we are using for spincoating is mica. Before spincoating, a blade is used to cleave the mica into thin sheets. By cleaving the mica, a very clean and flat surface is produced which is crucial to obtaining reproducible data. Another reason for the use of mica is that it is easy for polymer films to be floated off from the mica surface and onto a water surface by dipping into water.

The polymer used is polystyrene (PS) (purchased from Polymer Source Inc., Dorval Quebec, Canada) with M_w = 541,000, 785,400 and 1,410,000 (molecular weight quoted by the manufacturer, to be discussed later). All the polymers are monodisperse with a polydispersity index less than 1.1, as quoted by Polymer Source Inc. Solutions were made by dissolving PS into toluene, with mass fractions ranging from 0.50 to 4.00 %. In order to obtain homogeneous solutions, all the solutions were mixed for at least 24 hours prior to use in spincoating.

In this project, we used the 'drop-then-spin' method to produce films. The mica substrates used were 5 cm × 5 cm. The solution was dropped quickly onto the center of the substrate surface till the solution (~ 15 drops) covered at least ¾ of the substrate area. Then the stage for holding the substrate was spun at the speeds between 1500 and 6000 rpm. The film thicknesses, h, ranged from 30 nm to 700 nm, as measured by atomic force microscopy.

Preparation of a broad range of film thicknesses is very crucial in this project. The desired thickness was obtained by adjusting parameters such as mass concentration of the solution and the spinning speed. In table 2.1, we list the mass concentration of solutions, spinning speeds and film thicknesses for polystyrene with M_w = 785,400.

From this table, we can see that both the mass concentration and spinning speed were changed in order to obtain the film thicknesses required. When the mass concentration is higher than 1.5%, it was found to be difficult to spincoat films with uniform thickness over the large mica substrates. For high concentration solution, the acceleration rate was decreased in order to obtain more uniform films.

Table 2.1 Mass concentration, spinning speed and the resulting film thickness for PS with M_w = 785,400, dissolved in toluene of solution.

Mass Concentration of Solution (%)	Spinning Speed (rpm)	Film Thickness (nm)
3.00	4000	280
2.50	4000	213
2.00	3000	143
2.00	4000	115
1.75	4000	100
1.75	5000	90
1.50	4000	68
1.25	4000	54
1.00	3000	45
1.00	3500	42
1.00	4000	35

2.1.2 Annealing

After spincoating, the samples were put into a vacuum oven for annealing. The proper annealing conditions are important for us to study SDZ's in polymers. There are three reasons for annealing the films prior to use: 1) the polymer chains must be given enough time to achieve their equilibrium conformation (during the spincoating process, polymer chains may be aligned resulting in residual stresses which may affect the polymer properties. 2) to remove the remnant solvent molecules; and 3) to ensure a well-defined thermal history by cooling the samples at a given rate. The samples were annealed for at least 12 hours under vacuum with a temperature of 115 °C (~ 18°C above the glass transition temperature).

2.1.3 Preparation of free-standing films

After annealing, the samples were cooled at a rate less than 1 K/min and taken out of the oven at room temperature. A scalpel blade was used to cut the film into 1 cm × 1 cm squares (normally the weight of the scalpel was found to be enough to cut through the PS film, yet not cause too much mica dust on the samples). A water bath with very clean de-ionized water (Milli-Q) was used to float the film off the mica onto the water surface. The purity of the water is crucial for the experiment because the contaminants affect the nucleation of the shear deformation zone.

Using tweezers the PS/mica sample is slowly dipped into the water as shown in Figure 2.1. The PS films float on the water surface. Then the stretching holder is used to

pick up the film from the water surface as shown in Figure 2.2. Each time before picking up the films, the holder was cleaned with toluene to ensure no contamination to the water and films. The free-standing film on the stretching holder is dried in air for 15-20 min in a clean environment.

A few points regarding the transfer of the PS film to the sample holder should be noted. Normally a section of film which is close to the center of the mica substrate is used, because this section is most uniform. This is especially true for thick films. When floating off the film onto the water surface, we can see the presence of defects on the film as variations in color. Since the film is cut into many small pieces of square-shaped films, we can always find some defect free and uniform sections. In addition we were careful to pick up the film as soon as possible after floating onto the water, because the properties of the film *might* be changed by long exposure to water.

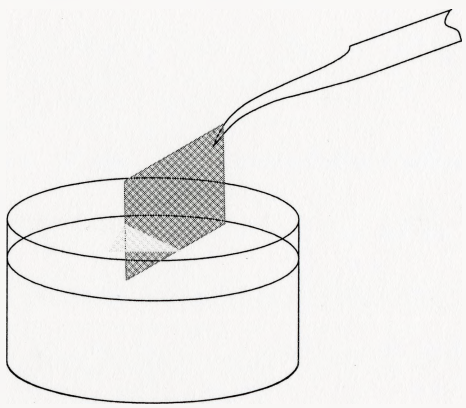

Figure 2.1 Floating the film off mica onto the water surface.

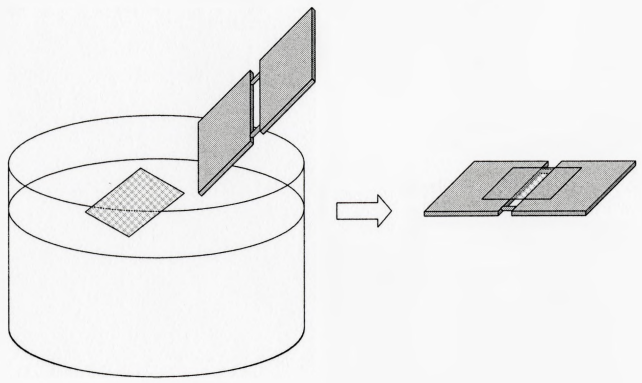

Figure 2.2 Pick up the film from water surface.

2.1.4 Stretching the film

After the film was prepared, the sample is mounted on the stretching system. The home built apparatus consists of three main parts (as shown in Figure 2.3): translation stage, motion controller, and microscope. The stretching holder was mounted on a translation stage as shown in Figure 2.4. The motion of the translation stage (Newport MFN25CC) is finely controlled by the controller (Newport ESP 300) and a computer. The controller can be operated manually, as well as through a computer. Labview was used to operate the controller (through GPIB interface) which in turn controls the motion of the translation stage. The speed and direction of the translation stage can be controlled fully through the custom made Labview program. The translation stage has a resolution of 0.055 μm.

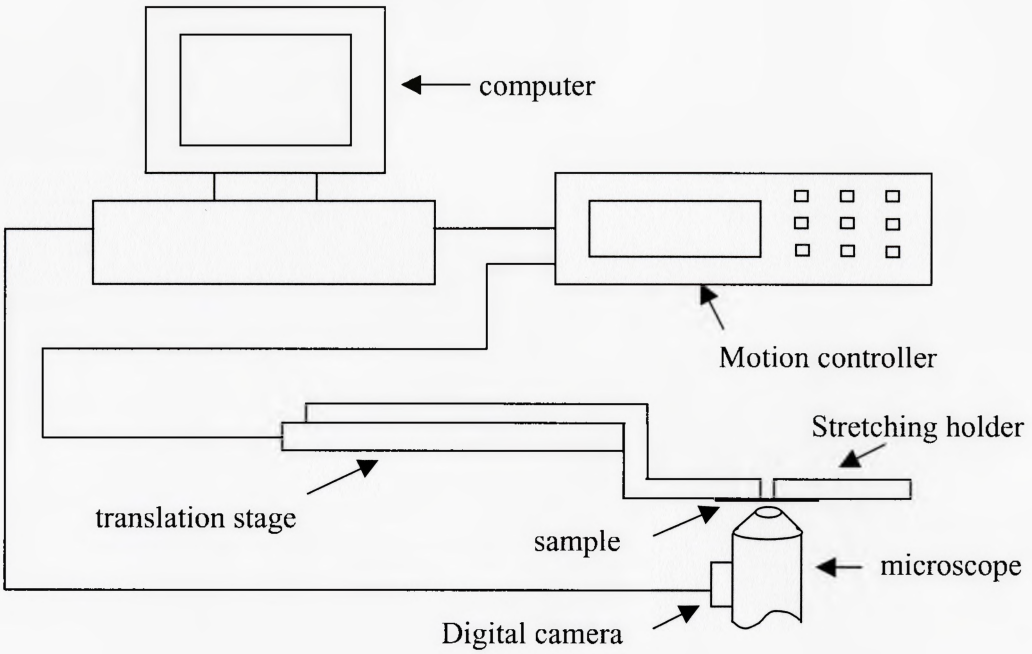

Figure 2.3 Schematic drawing of stretching system.

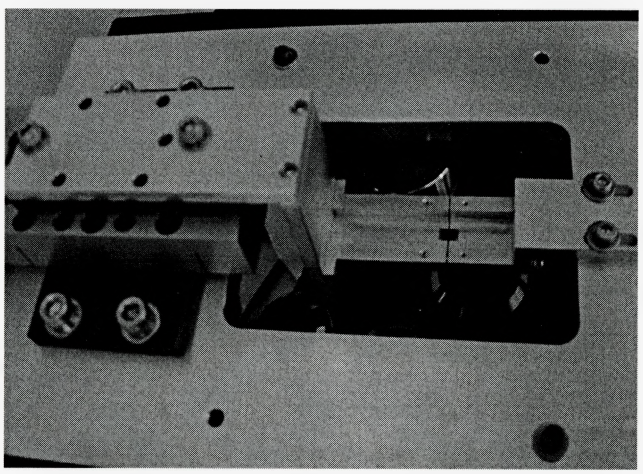

Figure 2.4 Translation stage and stretching holder.

The translation stage and sample holder are mounted on an optical microscope (as shown in Figure 2.5), so that the stretching process can be monitored optically. A digital camera is installed on the microscope, so that the shear deformation zone morphology can be captured. A sequence of images is taken so that a movie of the stretching process can be made.

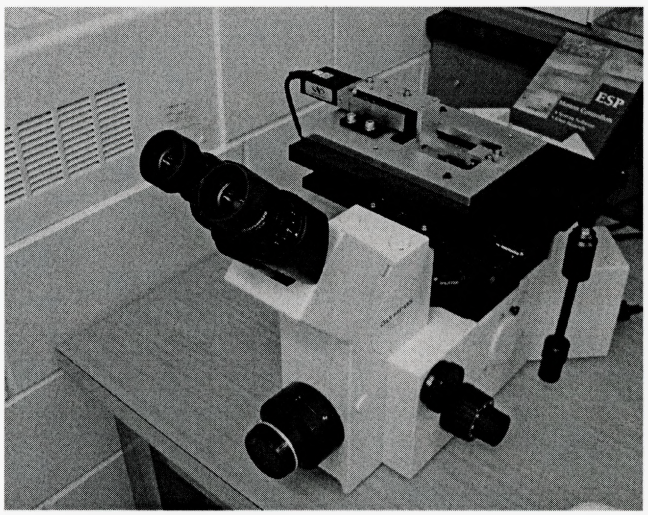

Figure 2.5 Optical microscope and stretching system.

2.1.5 The Labview program

Below we provide some detailed information about the Labview program and operation procedure. The main interface of the custom made Labview program is shown in Figure 2.6. The front panel shown in Figure 2.6 can be used to control the motion system precisely. First, some parameters are set: for example, in this project the fastest

speed is 0.3 mm/s and the slowest speed 0.0003 mm/s. For acceleration and deceleration rate, the default value of 1.2 mm/s^2 was used. The program is started by clicking the RUN button on the upper-left corner, and then clicking middle red button (Move axis 1 by a certain amount). A new panel will appear as shown in Figure 2.7. Where the distance the motor must move is entered. Then red button is clicked to make the motor move either in the negative direction or in the positive direction. During the stretching process, a cover is placed on the stretching holder to make sure the film is in a dust free environment.

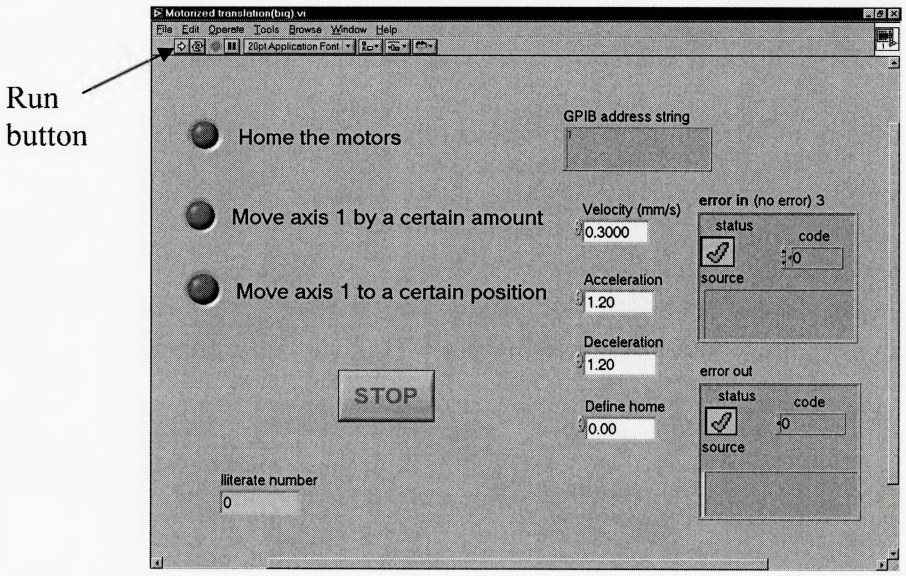

Figure 2.6 The main interface of Labview program for the motion system.

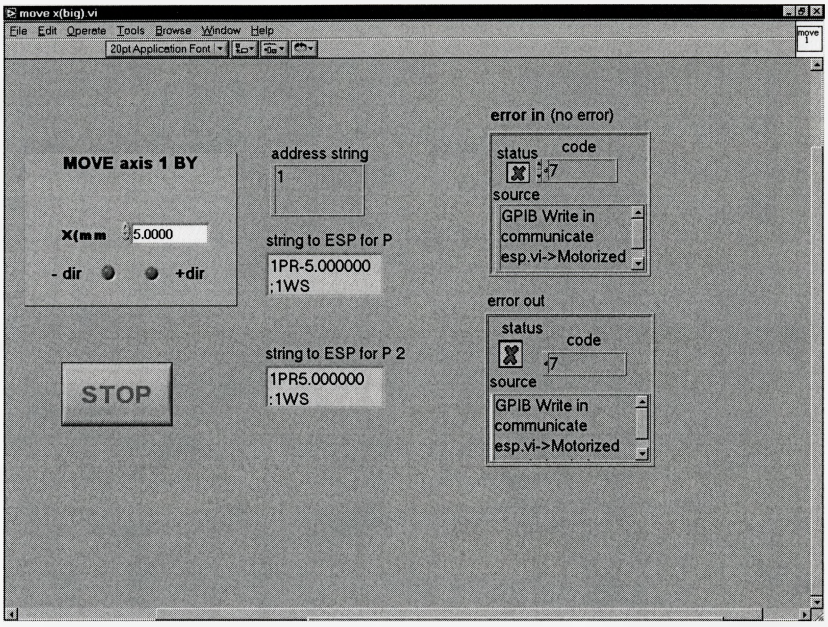

Figure 2.7 Labview interface for motion operation.

2.1.6 Transferring the stretched films onto the Si substrate

In order to characterize the shear deformation zones in the stretched films, the sample is transferred to a Si substrate, as shown in Figure 2.8. The stretching holder is placed onto the Si substrate and then a blade is used to cut the film, which is drawn onto the Si surface by van der Waals forces. Now the sample is ready for characterization by atomic force microscopy.

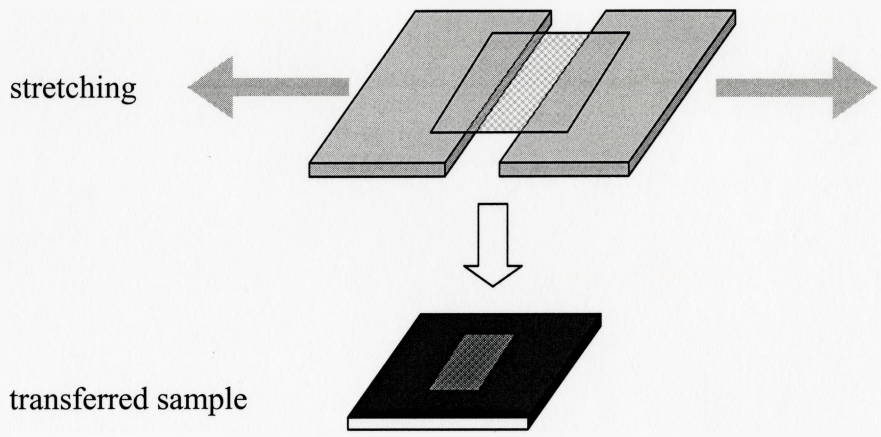

Figure 2.8 Transferring the stretched film onto Si substrate.

It is worth mentioning a problem that occurred during the transferring process. After stretching, the cross section of the stretched film at a shear deformation zone is a neck as shown in Figure 2.9a. After transferring the films onto the Si substrate, the neck of the film is pulled, by surface forces, onto the Si surface as shown in Figure 2.9b. For thin films the width of the neck is very large compared to the thickness of the neck and the geometry shown in Figure 2.9b is always observed. Typically the width of the neck is tens of microns while the neck is tens of nanometers. If the film is thin enough, the aspect ratio of width and thickness of the neck is about three orders of magnitude. Due to the van der Waals forces, this flexible neck is easily pulled onto the Si surface. However for relatively thick films (greater than $h \sim 500$ nm), the aspect ratio is not big enough, and the neck is not easily pulled to the substrate. We tried several ways to solve this problem. After stretching the film, the tension in the film was released a little and the neck could

be drawn to the substrate. In addition, before transferring the stretched film onto the Si substrate, we put one small drop of water on the Si surface, and placed the film on top. By doing so, the water helped to suck the neck onto the Si surface. These solutions were effective for wide shear deformation zones. For narrow necks, we could not have them deform onto the surface, but it was always possible to find some crazes that did have the configuration shown in Figure 2.9b.

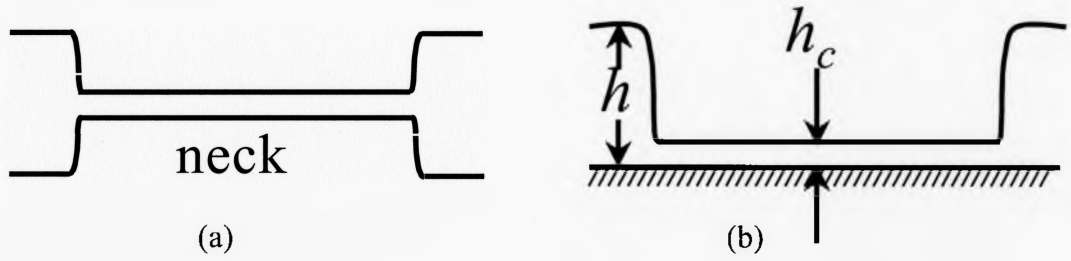

Figure 2.9 (a) Stretched film; (b) The film transferred onto Si substrate.

2.2 Sample characterization

The samples were characterized by optical microscopy and atomic force microscopy as described below.

2.2.1 Optical microscopy

Optical microscopy is a very useful tool for the characterization of polymers. Microscopy becomes especially powerful when coupled to a good digital camera and image processing software. In this project, optical microscope was used to monitor the necking process and take series of pictures, used to make a movie of the necking process.

2.2.2 Atomic force microscopy

Atomic force microscopy (AFM) was the main characterization tool used in this project.

2.2.2.1 Introduction to atomic force microscopy (AFM)

Atomic force microscopy offers the ability to perform high resolution profiling of surface morphology and nanostructure, and can provide information on local material properties and compositional mapping of samples. AFM has become an important method to examine materials, especially polymeric materials, such as engineering plastic, paints and coatings, rubber, packaging, fibers, and a wide range of consumer goods. Initially, AFM was used for observing polymer morphology, structure and molecular order. Novel applications of AFM are continuously being developed. In addition, the new technology makes AFM powerful not only in observation of top-most surface features, but also the underlying near surface sample structure.

The AFM is mainly composed of the following parts: the cantilever and tip, the piezoelectric scanner, and photodector as shown in Figure 2.10. The cantilever is flexible and the back surface is reflective. The tip is very small, with a radius of the curvature of about 5-10 nm. The piezoelectric scanner is used to give a 3-D scanning motion. The sample is put on the surface of piezoelectric scanner. So the sample is able to have a 3D motion. When the tip is close to the sample surface, the forces between the tip and surface will make the cantilever bend. A laser is shining on the back of the cantilever and

reflected onto a photodetector. Any vertical movement of the cantilever will change the laser position on the photodetector. The photodector collects all the signal of cantilever deflections and sends this to a computer. The computer will generate an image of the surface topography.

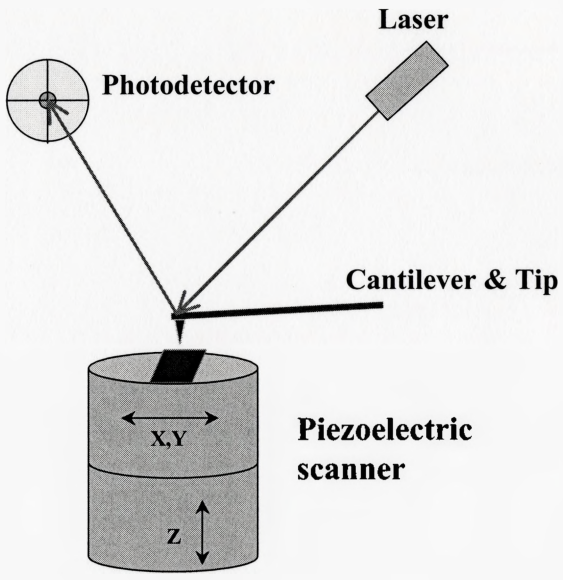

Figure 2.10 AFM imaging system.

Polymeric materials are relatively soft, therefore, imaging requires the force between the AFM tip and the sample surface to be as low as possible; to avoid damaging the polymer sample. Tapping mode AFM is able to meet with this requirement. This mode of AFM scans the sample surface by oscillating the AFM tip across the sample. In this way it can prevent damage by eliminating the lateral forces. Because of this special imaging, the tapping mode AFM is a very important technique for polymer studies. In this project, we used tapping mode AFM to characterize our polymer films. In addition, the tapping

mode AFM can also provide high height resolution information about surface profile and it could be better than 1 nm. This is very important for us because our main measurements by AFM are height measurements.

2.2.2.2 Method for thickness measurement

In this project, we used AFM to measure the film thickness and the thickness of the shear deformation zone. Although the resolution of height measurement for AFM is very high, it is easy to have some measurement errors if the method of measurement is not consistently and carefully executed. Here we provide detailed information about the measurements.

Before doing measurements, a blade is used to make some scratches which have an angle of about 45 degrees between the shear deformation zones and the scratches. The scratches go through the polymer film but do not penetrate the Si surface. AFM is used to image the stretched sample with some scratches on it. It is easy to have some extra polymer accumulated along the edge of scratches when scratching samples. If the extra polymer is too high, it will contaminate the AFM tip and also affect the accuracy of our measurements. In order to get accurate measurements, we tried to make the scratches as clean and thin as possible when scratching samples and tried to find a clean area to image.

Normally the shear deformation zone and scratch are imaged at the same time. Figure 2.11a is a typical image obtained from AFM. The dark color corresponds to a low level and the light color corresponds to a high level. So the darkest area is the scratch and

corresponds to the surface of the Si substrate. The lightest area is the film and the medium one is the neck.

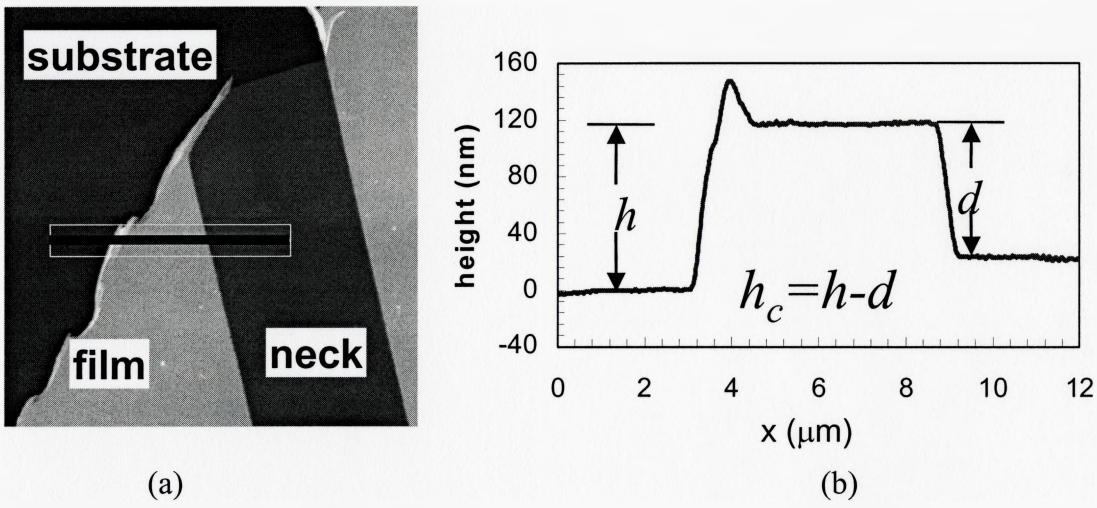

Figure 2.11 (a) AFM image; (b) Profile of the image.

The image must be carefully leveled, after which we can get the profile of the image as shown in Figure 2.11b. The area we choose to profile normally meets the following requirements. Firstly, each surface (film, neck and substrate surface) in the area is level. Secondly, each surface should be parallel to each other. Thirdly, we try to select the area in which the neck and substrate are as close as possible to each other. Based on this, we can choose an optimal area and measure the film thickness h and the neck thickness h_c at the same time as shown in Figure 2.11b.

Because the film is not absolutely uniform, especially for thick film, we take at least five AFM images for one sample. And for one image, we take at least five measurements which meet our three requirements mentioned above.

2.2.3 Gel Permeation Chromatography (GPC)

In this project, we used Gel Permeation Chromatography to measure the molecular weight of the polymers which were purchased from Polymer Source Inc. The molecular weight of the polymers we used for this project is very important, since it is directly related to fundamental parameters in the model. We found that there are deviations between our measurements and the values which were quoted by Polymer Source Inc. We have confidence in our measurements because we measured these three polymers at the same time with 6 calibration standards. The molecular weight for these polymers are listed in Table 2.2.

Table 2.2 Molecular weight comparisons between manufacturer's value and our measurements.

	Polymers	M_n	M_w	PI
Values from Polymer Source Inc.	#1	492,000	541,000	1.1
	#2	734,000	785,400	1.07
	#3	1,340,000	1,410,000	1.05
Our measurements	#1	577,408	624,000	1.08
	#2	694,043	828,000	1.19
	#3	909,884	1,062,000	1.17

Chapter 3 Results and discussions

3.1 Experimental results

In the following sections the experimental results obtained with optical microscopy and atomic force microscopy will be discussed.

3.1.1 Strain rate dependence of the ratio of the shear deformation zone thickness and the film thickness, h_d/h

In the experiments four different strain rates were used which ranged over 3 orders of magnitude: 2×10^{-1} s^{-1}, 2×10^{-2} s^{-1}, 2×10^{-3} s^{-1} and 2×10^{-4} s^{-1}. In order to test the scaling dependence of our data on the polymer molecular weight the experiments were performed with M_w = 1,062,000, 828,000, and 624,000. Here we first focus on the highest molecular weight used. The stretched films were examined by optical microscopy, and the typical morphology is shown in Figure 3.1. It was observed that the shear deformation zones appear qualitatively different under different strain rates. Typically high strain rates result in relatively narrow and densely distributed shear deformation zones (SDZ's), while for lower strain rates, there are fewer SDZ's that are wider. (see Figure 3.1).

In Figure 3.2 the ratio of the SDZ's thickness to the film thickness, h_c/h, is plotted for a series of measurements with four different strain rates and two sets of films with h = 40 nm and 120 nm. It is clear from the data that there is a reproducible difference between the different strain rates. The remaining scatter in the data is consistent with non-uniformity of the films. It can be seen that the ratio h_c/h is different for different film thicknesses and strain rates.

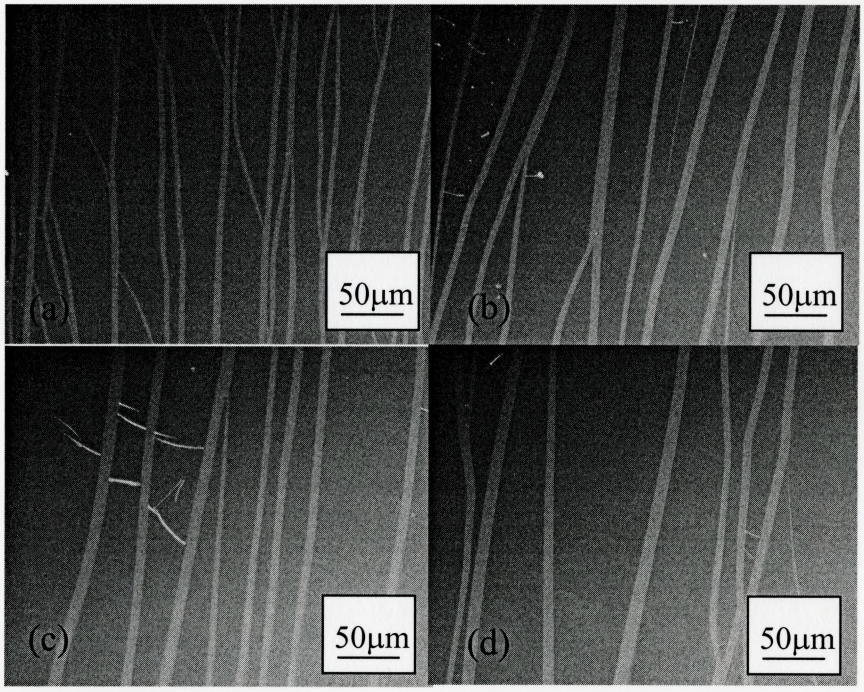

Figure 3.1 Typical SDZ morphology obtained by optical microscopy for different strain rates (a) 2×10^{-1}; (b) 2×10^{-2}; (c) 2×10^{-3}; (d) 2×10^{-4} s^{-1} (M_w = 1,062,000).

In order to clarify the dependence of h_c/h on the film thickness and the strain rate, the data in Figure 3.2 is averaged and plotted as a function of strain rate (see Figure 3.3). From this plot, it is obvious that the ratio h_c/h is strongly dependent on both the strain rate and the film thickness. The ratio h_c/h increases with increasing strain rate. The reason for this is that the polymer chains cannot re-arrange as efficiently when the strain rate is increased, resulting in a thicker SDZ and a larger ratio of h_c/h. In addition, it also can be seen in Figure 3.3, that, there is a clear dependence on the film thickness. For a given strain rate, the ratio h_c/h for the thicker film is higher than that of thinner film.

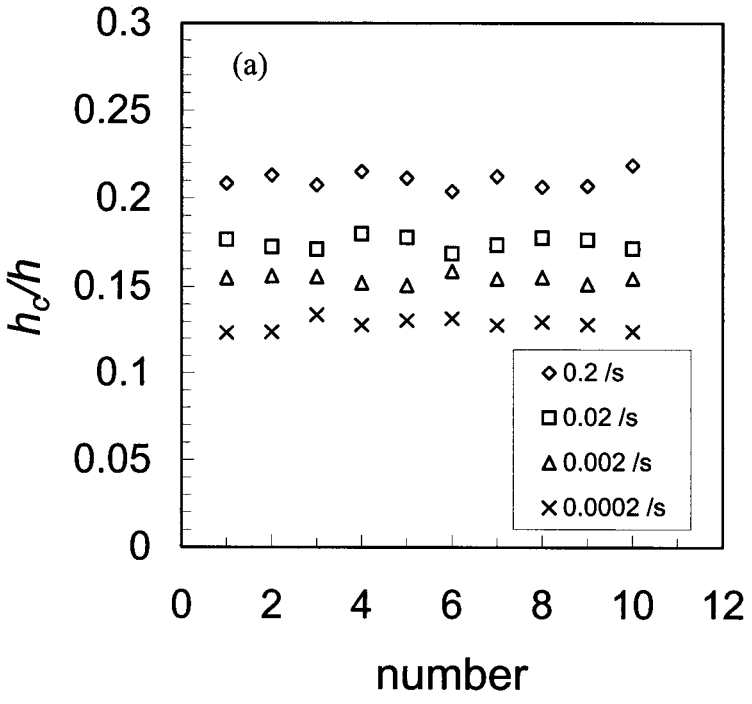

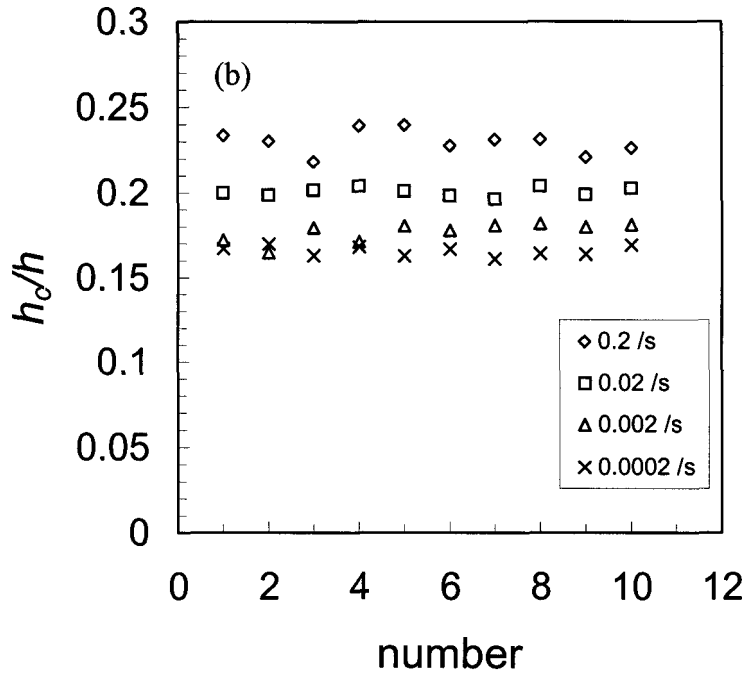

Figure 3.2 The ratio of h_c/h for a series of measurements with M_w = 1,062,000. (a) 40 nm film; and (b) 120 nm film.

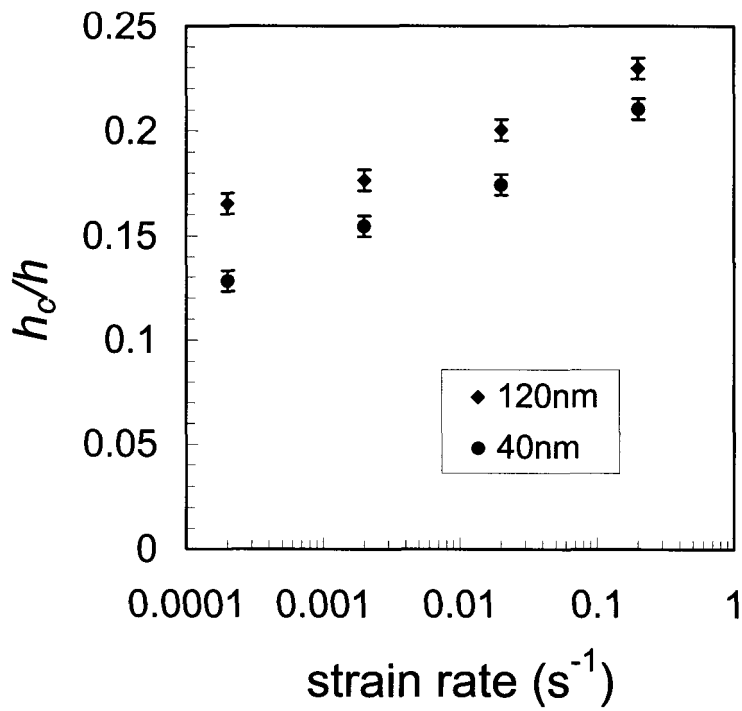

Figure 3.3 The plot of h_c/h as a function of strain rate for 40 nm and 120 nm films with M_w =1,062,000.

The main focus of the thesis was to investigate the relationship between h_c/h and the film thickness. In order to do this, a low strain rate (2×10^{-4} s^{-1}) was chosen for all experiments discussed hereafter.

3.1.2 Thickness dependence of h_c/h

In Figure 3.5 is shown a plot of the ratio h_c/h as a function of film thickness for different PS with M_w = 1,062,000; 828,000; and 624,000. From this plot we can see that for thick films a bulk value of h_c/h is obtained, while this ratio decreases with decreasing thickness below $h \sim 100$ nm, 70 nm and 60 nm for three different M_w's of PS: 1,062,000, 828,000, and 624,000 respecively (see Figure 3.4). Alternatively, the extension ratio $\lambda = (h_c/h)^{-1}$ increases with decreasing film thickness. The film thickness where we have a transition ($h \sim 100$ nm, 70 nm and 60 nm) is comparable to the end-to-end distance of the polymers used, R_{ee} = 76 nm, 67 nm and 58 nm indicating that the transition might be related to molecular size.

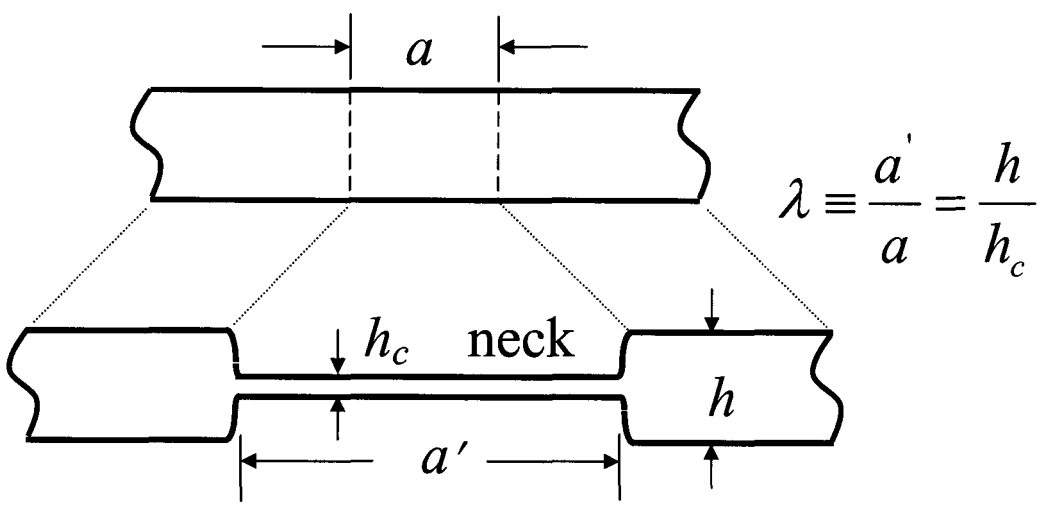

Figure 3.4 Schematic diagram of the stretched and un-stretched film and the extension ratio.

In Figure 3.5, it can also be seen that by decreasing the molecular weight, the data is scaled towards smaller film thickness indicative of a chain confinement effect. The data for the sample with low molecular weight shows more scatter in the thin film region. The reason is that since the decrease in h_c/h occurred for thinner films in the lowest molecular weights, it was necessary to perform measurements on thinner films and correspondingly thinner SDZ's. Measurements of thinner films with the AFM are susceptible to more noise. This was most apparent for films with thicknesses below $h \sim 40$ nm.

From Figure 3.5, the molecular weight dependence is clear. It might be expected that a chain-confinement effect scales with the end-to-end distance of the polymer ($R_{ee} \sim M_w^{1/2}$). Simply stated, a larger molecule is going to interact with the interfaces of a film for a larger film thickness than a smaller molecule. In Figure 3.6 we plot h_c/h as a function of h/R_{ee}. The data collapse onto a single master curve indicating that the decrease in the ratio h_c/h is the result of a chain confinement effect that scales with R_{ee}.

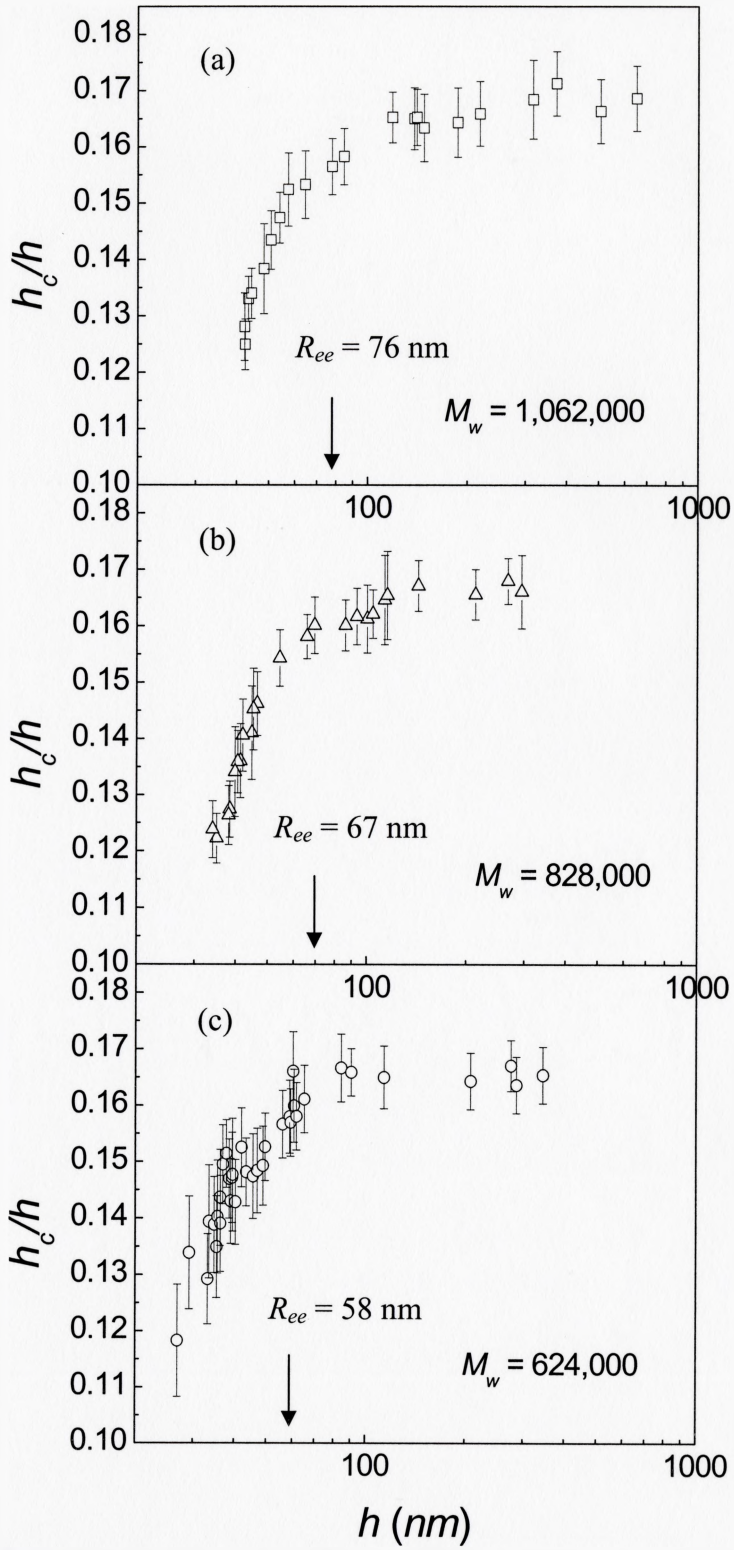

Figure 3.5 The plot of h_c/h as a function of h for different polymers with (a) M_w = 1,062,000; (b) M_w = 828,000; and (c) M_w = 624,000 respectively.

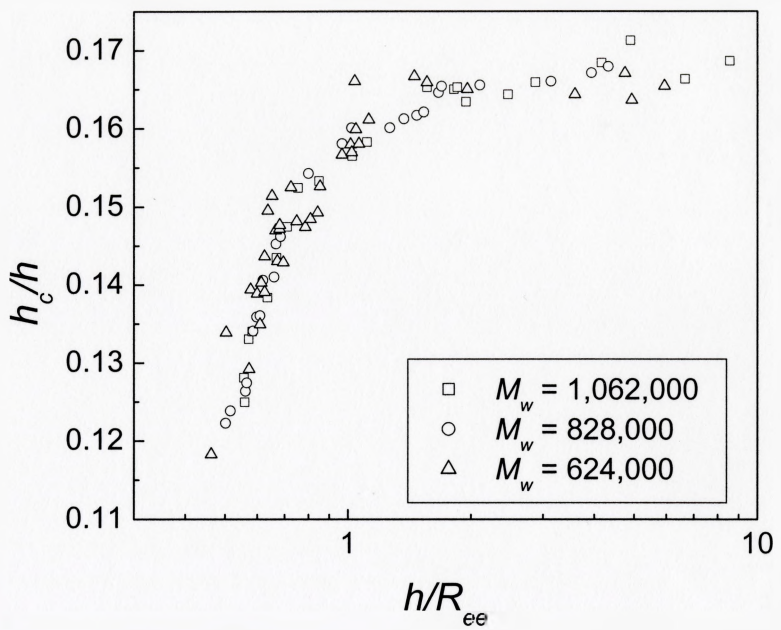

Figure 3.6 The plot of h_c/h as a function of h/R_{ee}.

3.1.3 Shear deformation zones and the entanglement molecular weight

In order to explain what happens to the film during the straining process, a simple model was developed by Kramer and co-workers [18]. The model is illustrated schematically in Figure 3.7.

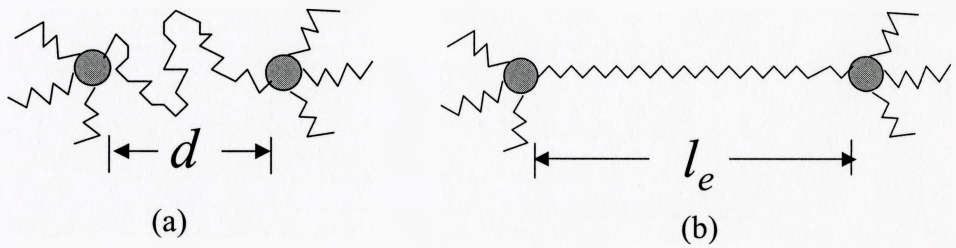

Figure 3.7 Schematic of a polymer chain between entanglements in (a) unstrained glassy polymer, and (b) the strained glassy polymer.

For unstrained film, the distance between entanglement points is d (see Figure 3.7a). After an applied strain, the maximum distance between entanglement points is the contour length of the chain l_e. If there is no slippage or breakage of the entanglement network points or the chains (i.e. the entanglement crosslinks act as permanent crosslinks), there will be a maximum extension ratio λ of the network given by

$\lambda = l_e/d.$

The contour length of the polymer chain between two entanglements scales like $l_e \sim M_e$, where M_e is the entanglement molecular weight. The unstrained film in equilibrium will execute a random walk between the entanglement points and the distance between entanglement points then scales like $d \sim (M_e)^{1/2}$. And if we assume that the density within the deformation zone is the same as that of the film and independent of film thickness, then $h_c/h = 1/\lambda = c/(M_e)^{1/2}$ (see Figure 3.4).

Based on this expression we see that a measure of the ratio h_c/h is a probe of the entanglement molecular weight. This then provides a way of interpreting the data shown in Figure 3.6. For thick films, a constant value of h_c/h is measured, which is proportional to the inverse of the entanglement molecular weight for PS. In the bulk, the entanglement molecular weight for PS is ~ 20,000. As the film thickness is decreased h_c/h decreases which implies a corresponding increase in the entanglement molecular weight. *While it cannot be claimed that thin films have a larger entanglement molecular weight (fewer crosslinks per unit volume), it is the case that thin films respond to a strain as if they were a material with fewer crosslinks.*

In this experiment it is not possible to differentiate between thin films having a lower entanglement density or thin films having entanglements which do not contribute to the integrity of the network. We define the effective entanglement molecular weight M_{eff} as the entanglement molecular weight which contributes to the integrity of the network. In Figure 3.8 the ratio of M_{eff}/M_e is plotted as a function of h. Clearly there is a significant increase in effective entanglement molecular weight when film thickness h is less than end-to-end distance R_{ee}.

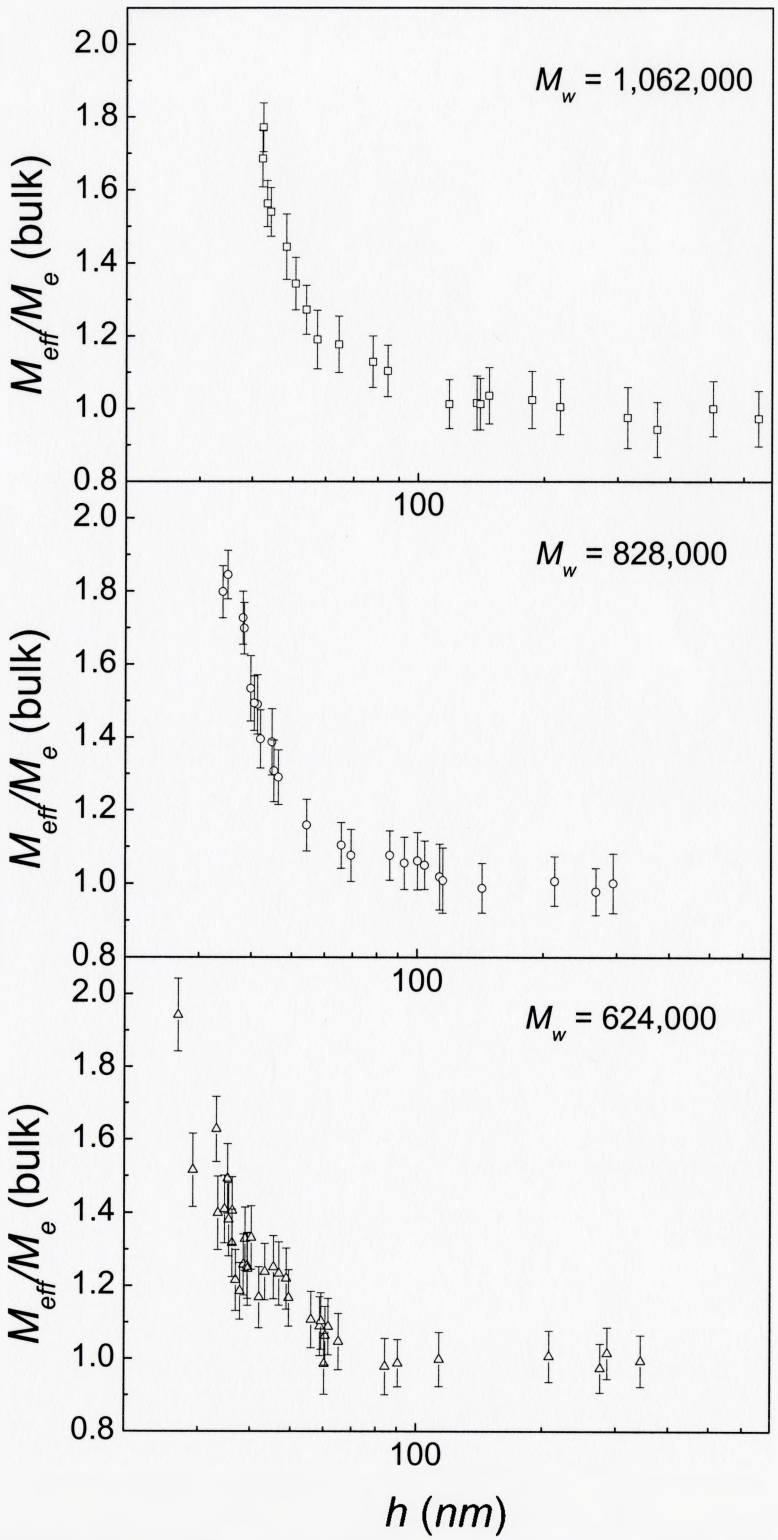

Figure 3.8 The plot of the ratio of effective entanglement molecular weight and entanglement molecular weight for bulk polymer as a function of film thickness.

3.2 Shear deformation model

The entanglement molecular weight for bulk polymers can be determined from measurements of the shear modulus of the melt in the rubbery plateau region just above the glass transition temperature T_g. However, to the best of our knowledge, there are no measurements of the entanglement molecular weight for thin polymer films. The data presented represent the first measurements which probe M_e in confined systems.

The data and analysis presented thus far are robust and rely on a few assumptions which are all well founded. In order to understand the mechanism for the reduced effective entanglement density in thin films, we present the following *tentative model.* One example of how some entanglements might be more effective than others is illustrated in Figure 3.9.

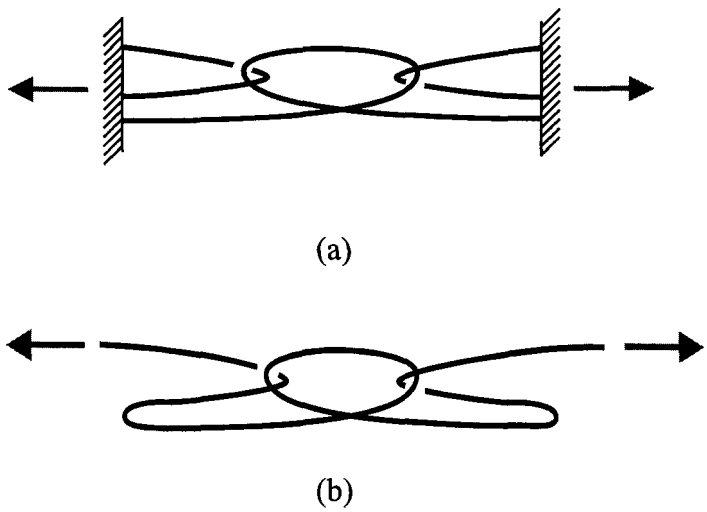

Figure 3.9 Schematic drawings of inter-chain and intra-chain entanglements.

From the figure it is quite obvious that the intra-chain entanglement and inter-chain entanglement are different. For the inter-chain entanglement (Figure 3.9a), it is not easy to stretch the chains far because the chains entangle with other chains. But for the intra-chain entanglement (Figure 3.9b), it is quite easy to stretch the chain out because only self-entanglements are involved.

As discussed above,

$$\frac{h_c}{h} = \frac{1}{\lambda} \sim \frac{1}{\sqrt{M_e}}. \qquad (1)$$

Here we assume that the density of the neck and the density of the film is the same. However, since large changes in the density are very unfavorable, even if there is a change in the density, this must be small. This expression can be generalized to the case of thin films by writing:

$$\left(\frac{h_c}{h}\right)^2 = \frac{1}{M_{eff}} \sim \nu_{eff}, \qquad (2)$$

where ν_{eff} is the effective entanglement density.

We need to address why the effective entanglement density might be different in thin films. As pointed out by de Gennes [31] in the thin film limit, chains exclude each other, and there are no entanglements with other chains. This is simply the result of the fact that a Gaussian chain can be represented by a random walk. For a random walk, the steps in the lateral dimensions of the film are not affected, whereas the steps in the

normal direction are limited to the film [27]. As the film thickness is decreased then chains need to be excluded from each other in order to avoid building up a density that is too high. In the thin film limit most of the entanglements are intra-chain entanglements and clearly a film made up of excluded chains would simply fail under a strain rather than form a SDZ. This necessarily implies that entanglements with other chains are important to the formation of a SDZ. With this model in mind, it is clear that increased intra-chain entanglements result in an increase in the effective entanglement molecular weight.

Now let us assume that the effective entanglement density is that fraction of the total entanglements of a chain that are with other chains, that is, inter-chain entanglements. So we can write

$$\nu_{eff} = \nu \cdot P_{inter}; \qquad (3)$$

where P_{inter} is the probability of an inter-chain entanglement, and ν is the total entanglement density. Since P_{inter} = 1- P_{intra}, the effective entanglement density is:

$$\nu_{eff} = \nu(1 - P_{intra}). \qquad (4)$$

Within this model, this is true for the bulk as well. The volume pervaded by the chain is defined as some volume within which a chain in the bulk interacts with other chains. From Figure 3.10, we can see that the volume pervaded by a chain inside the film is different from the volume pervaded by a chain at interface. For example, imagine that the centre-of-mass of a chain gets close to the interface. The interface represents a reflective boundary condition- i.e. a random walk is reflected back into the film [27].

That means that the volume at the interface is half of the volume in the bulk of the film. Since the *effective* entanglement density depends on the probability that an entanglement is with another chain, the entanglement density is different in the middle of the film from the near interface region. Since the SDZ experiment probes the entire film, we need to make the simplifying assumption that we can average the effective entanglement density ν_{eff} over the film thickness. In fact, ν_{eff} is lower near an interface, because that is where the pervaded volume of chain is perturbed. If the chain's pervaded volume in confinement were half that of an unperturbed chain, then the probability of a self-entanglement would be twice as high, i.e. $2P_{intra}$. In general we can write:

$$\nu_{eff} = \nu\left(1 - P_{intra}\frac{V_b}{V_p}\right) \qquad (5)$$

where V_b is the pervaded volume of the chain in the bulk and V_p is the pervaded volume of a chain in confinement. (see Figure 3.10)

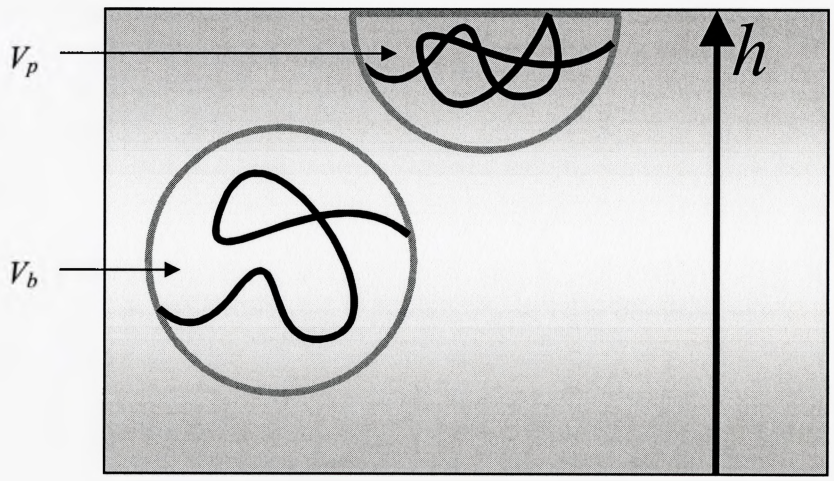

Figure 3.10 Pervaded volume of a chain in bulk polymer and near the interface.

We take the pervaded volume of a chain in the bulk to be

$$V_p = \frac{4}{3}\pi R^3,$$

where the radius of the pervaded volume scales with the end-to-end distance of a polymer molecule: $R = c \cdot R_{ee}$.

Averaging the effective entanglement density over the film thickness, we can rewrite equation (5) as:

$$\left\langle \nu_{eff} \right\rangle = \nu\left(1 - P_{intra}\left\langle \frac{V_b}{V_p} \right\rangle\right)$$

$$= \nu\left(1 - \frac{P_{intra}}{h}\int_0^h \frac{V_b}{V_p(x)}dx\right).$$

The key point here is to solve the integral for ratio of V_b/V_p. We define a dimensionless value of the film thickness, $H = h/R$. In order to calculate the average value of the effective entanglement density, there are three independent cases that are most easily handled separately.

Case 1: $H > 2$

Case 2: $1 < H < 2$

Case 3: $H < 1$

Case 1 and 3 are most easy to calculate, so we will start with these two cases.

Case 1: $H > 2$

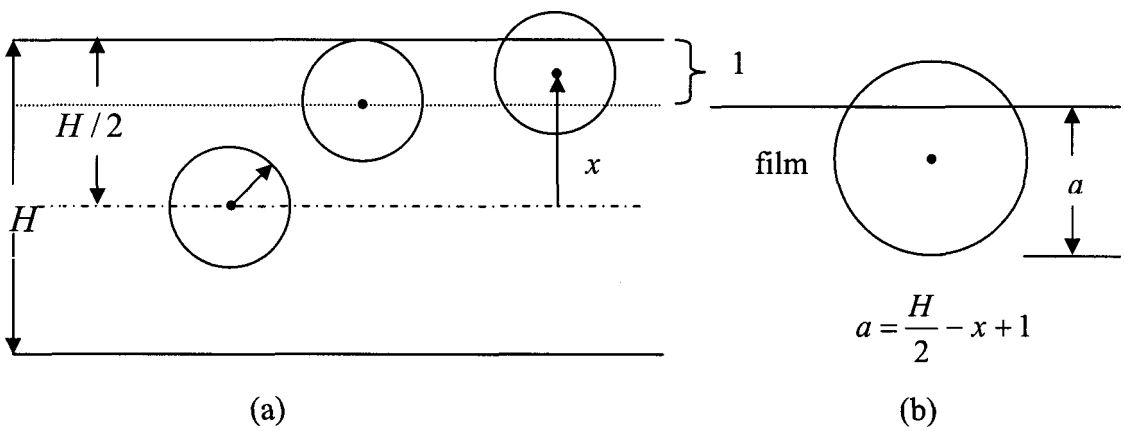

Figure 3.11 (a) The pervaded volume of the chain is located in the film with the film thickness $H > 2$; (b) pervaded volume of the chain is the volume of the portion of the sphere that is within the film boundary.

When the chain is located inside of the polymer film and has no contact with the film boundary, the volume pervaded by a chain is $V_b = \frac{4}{3}\pi R^3$. If the chain intersects with film boundary, the volume pervaded by a chain should equal the volume of the sphere inside of the film, that is, $V_p^{'} = V_{cap}$. The volume the of cap is $V_{cap} = \frac{1}{3}\pi a^2(3R - a)$, where $a = \frac{H}{2} - x + 1$, is the height of the cap, as shown in Figure 3.11b. We have the following integral:

$$\left\langle \frac{V_b}{V_p} \right\rangle = \frac{2}{H}\int_0^{\frac{H}{2}} \frac{V_b}{V_p}\,dx = \frac{2V_b}{H}\underbrace{\left(\int_0^{\frac{H}{2}-1} \frac{dx}{V_p}\right)}_{A} + \underbrace{\int_{\frac{H}{2}-1}^{\frac{H}{2}} \frac{dx}{V_p}}_{B}$$

$$A = \int_0^{\frac{H}{2}-1} \frac{dx}{V_p} = \frac{3}{4\pi}\int_0^{\frac{H}{2}} dx = \frac{3}{8\pi}(H-2)$$

$$B = \int_{\frac{H}{2}-1}^{\frac{H}{2}} \frac{dx}{V_{cap}} = \int_{\frac{H}{2}-1}^{\frac{H}{2}} \frac{dx}{\frac{1}{3}\pi a^2(3-a)} = \frac{1}{6\pi}(4\ln 2 + 3)$$

$$\left\langle \frac{V_b}{V_p} \right\rangle = \frac{2V_b}{H}\left[\frac{3}{8\pi}(H-2) + \frac{1}{6\pi}(4\ln 2 + 3)\right]$$

$$= \frac{V_b}{\pi H}\left(\frac{3}{4}H + \frac{8\ln 2 - 3}{6}\right)$$

$$= \frac{V_b}{\pi}\left(\frac{3}{4} + \frac{0.4242}{H}\right)$$

Therefore, when $H > 2$, it is easy to show that

$$\left\langle \nu_{eff} \right\rangle = \nu\left[1 - \frac{P_{intra}\cdot V_b}{\pi}\left(\frac{3}{4} + \frac{0.4242}{H}\right)\right]$$

$$= \nu\left[1 - P_{intra}\cdot\frac{4}{3}\left(\frac{3}{4} + \frac{0.4242}{H}\right)\right],$$

$$\left\langle \nu_{eff} \right\rangle = \nu\left[1 - P_{intra}\left(1 + \frac{4}{3}(0.4242)\cdot\frac{R}{h}\right)\right].$$

Case 3: $H<1$

When $H<1$, the sphere has to intersect with two film boundaries at all times as shown in Figure 3.12.

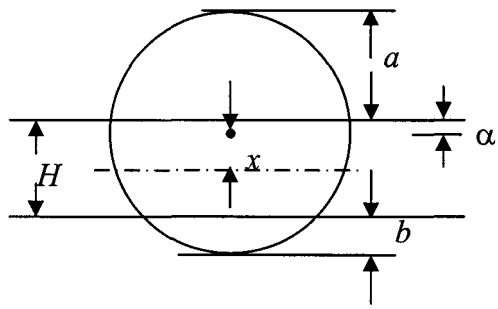

Figure 3.12 The sphere intersect with two interfaces of the film when $H<1$.

We can start the integral from center of the film. If the sphere starts to move up from the center of the film, then the height of upper cap outside of the film is a and the height of the lower cap is b. a and b are given by

$$a = 1-\alpha = 1-\frac{H}{2}+x$$

$$b = 2-a-H = 1-\frac{H}{2}-x$$

So we can write the integral as follows:

$$\left\langle \frac{V_b}{V_p} \right\rangle = \frac{2}{H}\int_0^{\frac{H}{2}} \frac{V_b}{V_p}\,dx$$

$$V_p = \frac{4}{3}\pi - V_{cap,a} - V_{cap,b}$$

$$= \frac{4}{3}\pi - \frac{1}{3}\pi a^2(3-a) - \frac{1}{3}\pi b^2(3-b)$$

$$= \pi H\left(1 - \frac{H^2}{12} - x^2\right)$$

$$\left\langle \frac{V_b}{V_p} \right\rangle = \frac{2V_b}{H}\int_0^{\frac{H}{2}} \frac{dx}{\pi H\left(1 - \frac{H^2}{12} - x^2\right)}$$

$$= -\frac{12V_b}{H} \cdot \arctan\left[\frac{3H}{\sqrt{-36+3H^2}}\right] \cdot \left[\pi H\sqrt{-36+3H^2}\right]^{-1}$$

Therefore, when $H < 1$, the average effective entanglement density is given by

$$\langle \nu_{eff} \rangle = \nu\left\{1 + P_{intra}\left[\frac{12V_b}{H} \cdot \arctan\left[\frac{3H}{\sqrt{-36+3H^2}}\right] \cdot \left[\pi H\sqrt{-36+3H^2}\right]^{-1}\right]\right\}$$

Now let's see the extreme situation of an ultra-thin film. When H is approaching zero, that means film thickness is very small, the pervaded volume of a chain in this confinement would be the volume of the small cylinder with radius R within the film. This is given by

$V_p = \pi R^2 h$, and the ratio of V_b/V_p is

$$\frac{V_b}{V_p} = \frac{\frac{4}{3}\pi R^3}{\pi R^2 h} = \frac{4}{3}\frac{R}{h} = \frac{4}{3}\frac{1}{H}.$$

So when $h << R$ ($H << 1$), the average effective entanglement density will be

$$\langle \nu_{eff} \rangle = \nu\left(1 - P_{intra} \cdot \frac{4}{3}\frac{R}{h}\right).$$

Case 2: $1 < H < 2$

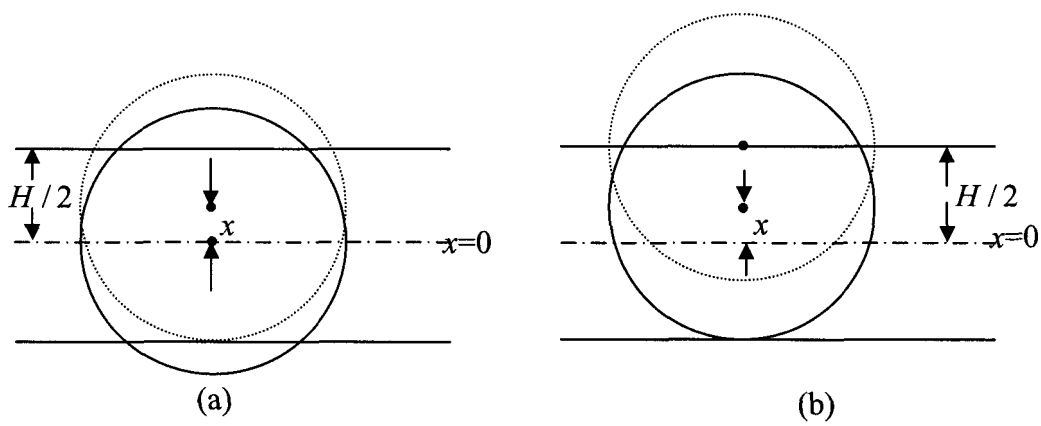

Figure 3.13 There are two cases when $1 < H < 2$: (a) the sphere intersects with two interfaces; (b) the sphere intersects with one interface.

This is the most complicated case because there are two situations. The sphere can intersect with one or two interfaces (see Figure 3.13).

Suppose the mass center of the sphere is located in the center of the film. There are two caps which have same volume. Then we start to integrate from center of the film to x, where the sphere just starts to intersect with one interface as shown in Figure 3.13. Here $x = 1 - \frac{H}{2}$. In the other situation, we continue to integrate from the point where the sphere just starts to intersect with one interface to the point where the mass center is on the film interface.

Therefore, the integral ranges for two situations are listed as following:

2 caps: $0 < x < 1 - \frac{H}{2}$

1 cap: $1-\frac{H}{2}<x<\frac{H}{2}$

The integral is given by

$$\left\langle \frac{V_b}{V_p} \right\rangle = \frac{2V_b}{H}\left(\underbrace{\int_0^{1-\frac{H}{2}} \frac{dx}{V_p^{'}}}_{A} + \underbrace{\int_{1-\frac{H}{2}}^{\frac{H}{2}} \frac{dx}{V_p^{''}}}_{B} \right)$$

The pervaded volumes of the chain $V_p^{'}$ and $V_p^{''}$ are same as the volume which we calculated in case 3 and 1.

$$V_p^{'} = \pi H\left(1-\frac{H^2}{12}-x^2\right)$$

$$V_p^{''} = \frac{1}{3}\pi a^2(3-a)$$

$$A = \int_0^{1-\frac{H}{2}} \frac{dx}{\pi H\left(1-\frac{H^2}{12}-x^2\right)}$$

$$= 6\cdot \arctan\left[3\frac{H-2}{\sqrt{-36+3H^2}}\right]\cdot\left[\pi H\sqrt{-36+3H^2}\right]^{-1}$$

$$B = \int_{1-\frac{H}{2}}^{\frac{H}{2}} \left[\frac{1}{3}\pi a^3(3-a)\right]^{-1} dx\ ;\ a = \frac{H}{2} - x + 1$$

$$B = \frac{1}{3}\cdot\frac{H\ln 2 + 3H + iH\pi + H\ln H - 3 - H\ln(H-3)}{\pi H}$$

Since $\ln(-1) = i\pi$,

$$B = \frac{1}{3}\cdot\frac{H\ln 2 + 3H + H\ln(-1) + H\ln H - 3 - H\ln(H-3)}{\pi H}$$

$$= \frac{1}{3\pi H}\left[H\ln\left(\frac{2H}{3-H}\right) + 3(H-1)\right]$$

$$\left\langle\frac{V_b}{V_p}\right\rangle = \frac{2V_b}{H}\left\{6\cdot\arctan\left[(3H-6)(-36+3H^2)^{\frac{1}{2}}\right]\cdot\left[\pi H(-36+3H^2)^{\frac{1}{2}}\right]^{-1}\right.$$

$$\left. + \frac{1}{3\pi H}\left[H\ln\left(\frac{2H}{3-H}\right) + 3(H-1)\right]\right\}$$

$$\left\langle\frac{V_b}{V_p}\right\rangle = \frac{2V_b}{\pi H^2}\left\{6\arctan\left[(3H-6)(-36+3H^2)^{-\frac{1}{2}}\right]\cdot(-36+3H^2)^{-\frac{1}{2}}\right.$$

$$\left. + \frac{H}{3}\ln\left(\frac{2H}{3-H}\right) + H - 1\right\}$$

$$\nu_{eff} = \nu\left(1 - P_{intra}\cdot\left\langle\frac{V_b}{V_p}\right\rangle\right)$$

$$= \nu - \frac{2\nu P_{intra}V_b}{\pi H^2}\left\{6\arctan\left[(3H-6)(-36+3H^2)^{-\frac{1}{2}}\right]\cdot(-36+3H^2)^{-\frac{1}{2}}\right.$$

$$\left. + \frac{H}{3}\ln\left(\frac{2H}{3-H}\right) + H - 1\right\}$$

3.3 Model results

Now we have derived the expression of the average volume pervaded by a chain V_p. From the derivation of the simple model, we have

$$\left(\frac{h_c}{h}\right)^2 \sim \nu_{eff} = \nu\left(1 - P_{intra}\left\langle\frac{V_c}{V_p}\right\rangle\right)$$

Finally we can get the following relationship:

$$\left(\frac{h_c}{h}\right)^2 \sim \begin{cases} \nu\left[1 - P_{intra}\left(1 + \frac{4}{3}(0.4242)\cdot\frac{1}{H}\right)\right] & H > 2 \\ \nu - \frac{2\nu P_{intra} V_b}{\pi H^2}\left\{6\arctan\left[(3H-6)(-36+3H^2)^{-\frac{1}{2}}\right]\cdot(-36+3H^2)^{-\frac{1}{2}}\right. & \\ \left. + \frac{H}{3}\ln\left(\frac{2H}{3-H}\right) + H - 1\right\} & 1 < H < 2 \\ \nu\left\{1 + P_{intra}\left[\frac{12V_b}{H}\cdot\arctan\left[\frac{3H}{\sqrt{-36+3H^2}}\right]\cdot\left[\pi H\sqrt{-36+3H^2}\right]^{-1}\right]\right\} & \\ & H < 1 \end{cases}$$

where ν, V_c and P_{intra} are constants.

We plot the model result of $(h_c/h)^2$ as a functions of R/h, shown in Figure 3.14. From this simple scaling model, we can see that the model result follows a curve in which

$(h_c/h)^2$ decreases with the decreasing thickness of the film. In addition there are two regimes with a broad transition region centered at R/h = 1.3. For the regime in the left region of Figure 3.14, h is high (thick film) and the two spheres are not interacting each other. With decreasing film thickness, the two interfacial regions (with thickness R) will interfere with each other and amplify the effect of confinement. That is where the behavior switches to a steeper slope.

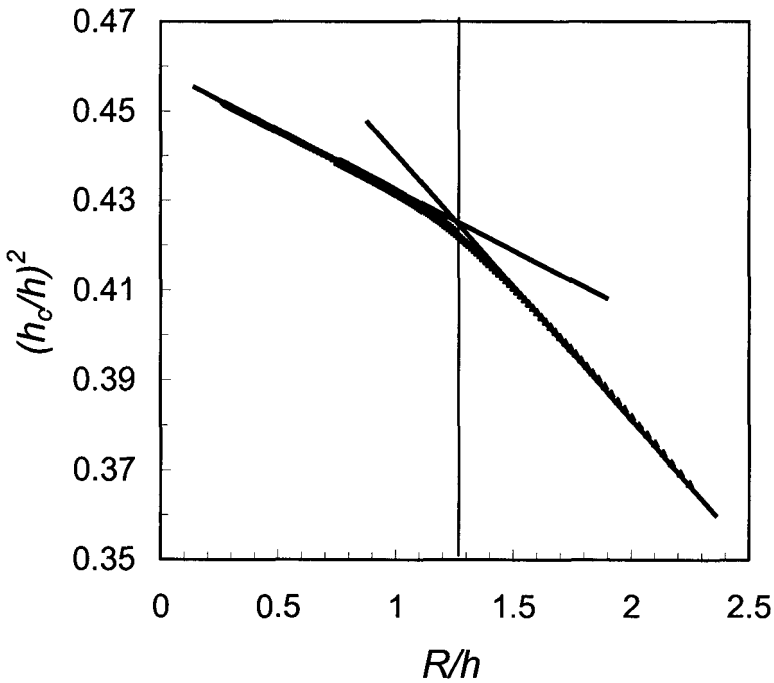

Figure 3.14 The plot of $(h_c/h)^2$ as a function of R/h (model result).

We also plotted $(h_c/h)^2$ as a function of $1/h$ for our experiment data with three different molecular weight as shown in Figure 3.15. It can be seen that there is a clear kink in the data when R_{ee} is roughly equal to $1.3h$ (see Figure 3.15a and b). This is exactly same behavior as that observed in the model. For Figure 3.15c, it is hard to see the kink because of the data scatter.

In Figure 3.16, we plotted $(h_c/h)^2$ as a function of R_{ee}/h for three different molecular weight. In Figure 3.16a is shown the plot for the two highest molecular weight. It is obvious that these two sets of data follow each other very well and follows closely the predictions of the model. In Figure 3.16b, the plot for all three molecular weight is shown. Comparing the Figure 3.16a and b, we can see that the experimental results for two highest molecular weight agree with the model result very well. For the lowest molecular weight, as we mentioned before, the data is scattered due to the non-uniformity when the thickness is less than 40 nm.

We can compare the experimental data with the model result in a more quantitative manner. We can find that the R is roughly equal to R_{ee}. We emphasize that the pervaded volume of a polymer chain is a theoretical construct useful in the understanding of polymer physics – within the assumptions made in this simple model, it turns out that this is a measurable quantity. Because there are some arbitrary prefactors relating to the slopes, we cannot compare the slopes of the model to that of the data directly. However we are able to compare the slope contrast between them. For model result, the slope contrast is 2.3. For data, the slope contrast is 3.1.

We emphasize that this is a tentative model which requires further development. However, the model is based on reasonable assumptions and predicts correctly the behavior of the data for all three molecular weights studied. More impressive is the fact that the model predicts a scaling of the data with R_{ee}/h. When all the data is plotted as a function of R_{ee}/h there is a universality that provides some confidence in the model and the interpretation of the data. It is a remarkable result that stretching a film can provide a

measure of the entanglement molecular weight of a thin film – a property that is difficult to measure in the bulk and has never before been probed in confinement. It is equally remarkable that such a simple measurement combined with the model quantifies the pervaded volume of a polymer chain.

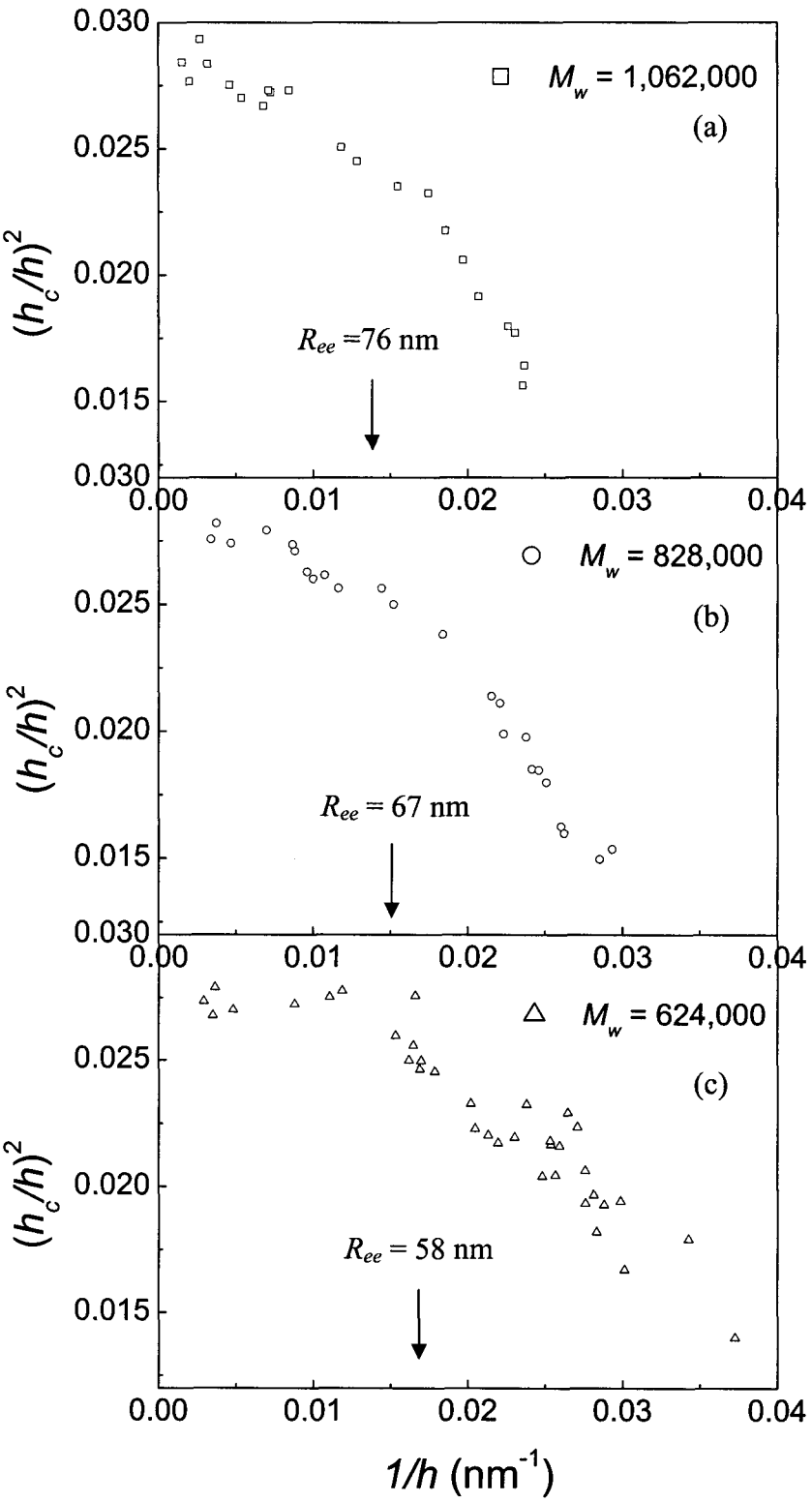

Figure 3.15 The plot of $(h_c/h)^2$ as a function of $1/h$ for experimental data.

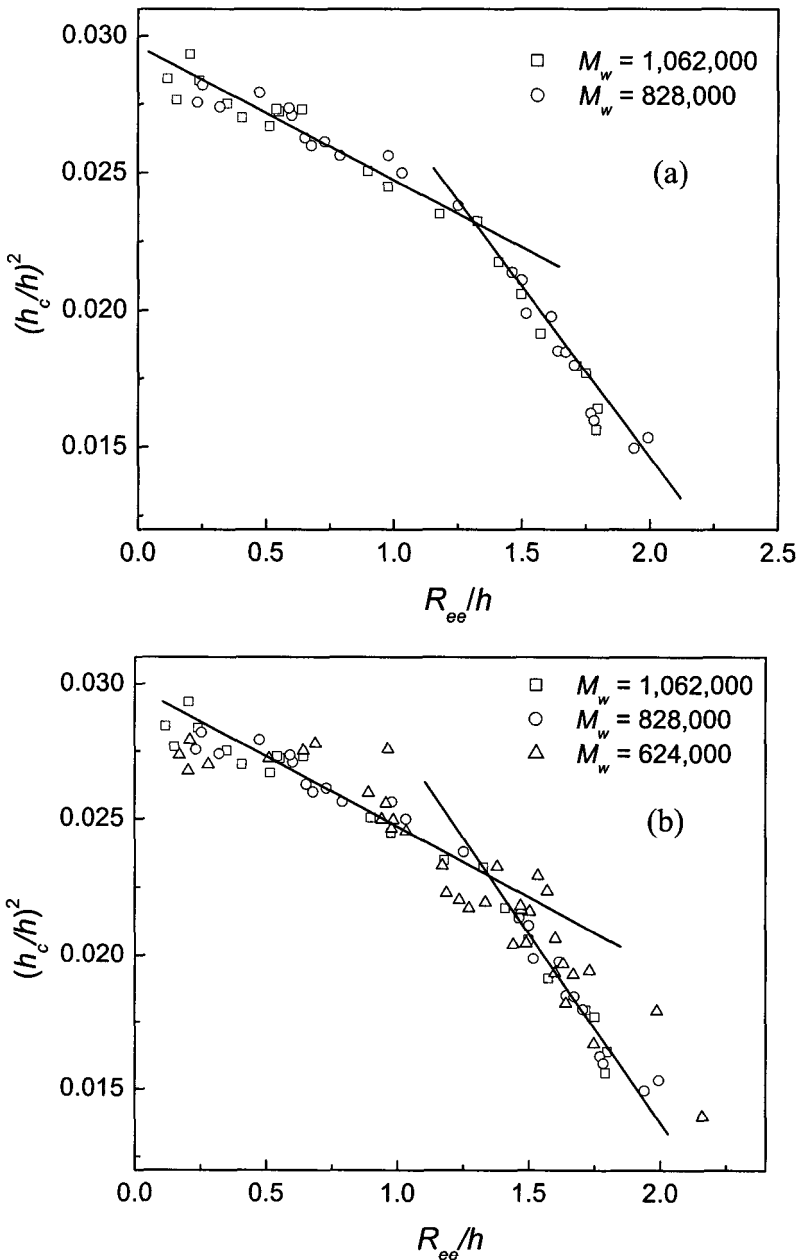

Figure 3.16 The plot of $(h_c/h)^2$ as a function of R_{ee}/h for different molecular wight: M_w = 1,062,000, 828,000, and 624,000. (a) The two highest molecular weights; (b) All three molecular weight.

Chapter 4 Conclusion

In this project we used deformation under uniaxial strain to investigate the entanglement in thin polymer films. We established a stretching system which can be automatically controlled by a computer. Various thicknesses of polystyrene films were prepared by spin coating. After annealing and floating off the films onto the water bath, the films were picked up by the stretching holder; and subsequently stretched under uniaxial stress. The deformed films were transformed onto the Si substrate for thickness measurements. By using atomic force microscopy (AFM), a large amount of measurements were done on the thickness of shear deformation zones (SDZ's) h_c and the film thickness h.

The measurements showed that the ratio h_c/h is dependent on strain rate. Higher strain rate will result in higher h_c/h. The ratio of h_c/h is also correlated to the thickness of the film. For thick film (or bulk polymer), the ratio is constant. For thin films, the ratio decreases with decreasing film thickness. The point where the ratio starts to decrease is comparable to the end-to-end distance R_{ee}. While it cannot be claimed that thin films have a larger entanglement molecular weight (fewer crosslinks per unit volume), it is the case that thin films respond to a strain as if they were a material with fewer crosslinks. Further experimental results indicated that the ratio of h_c/h is dependent on the molecular weight.

The plot of the effective entanglement molecular weight M_{eff} as a function of film thickness h showed that the effective entanglement molecular weight M_{eff} increased for thin films. The measure of the ratio h_c/h is a probe of the entanglement molecular weight.

A tentative model was developed. In this model, we assume that the density of SDZ and unstrained film are the same. And the inter-chain entanglement and intra-change entanglement are different. Based on this assumption, we can show that the effective entanglement density v_{eff} is proportional to $(h_c/h)^2$. By integrating v_{eff} over the whole film, we can get the average effective entanglement density $<v_{eff}>$. The model results showed that there is a transition where the slope in the plot of $(h_c/h)^2$ vs. R/h changed when R is roughly equal to $1.3h$. The change in the slope occurs because the chain can only touch one interface in a thick film but it can touch both interfaces in thin film.

Comparing the model result with the experimental results, we found that there is a good agreement between the simple model and the experimental data. If the tentative model developed is valid, then it is truly remarkable that we can provide a measure of the entanglement molecular weight in confinement, simply by stretching a film!

Reference:

[1] Eisele U., *Introduction to Polymer Physics* (Springer-Verlag Berlin Heidelberg, 1990).

[2] Callister W. D, Jr., *Fundamentals of Materials Science and Engineering* (John Wiley & Sons, Inc. 2001).

[3] Dalnoki-Veress K., *Confinement Effects on Thin Polymer Films*, Ph. D. Thesis, (University of Guelph, 1998)

[4] Gedde U. W., *Polymer Physics* (Chapman & Hall, 1995).

[5] Lauterwasser B.D., Kramer E.J. Phil. Mag. A39, 469 (1979).

[6] Kambour R.P., J. Polym. Sci. Macromol. Rev., 7, 1 (1973).

[7] Lainchbury D.L.G, Bevis M., J. Mater. Sci., 11, 2222 (1976).

[8] Argon A.S., Andrew R.D., Godrick J.A., Whitney W., J. Appl. Phys., 39, 1899 (1968).

[9] Kramer E.J., J. Macromol. Sci. Phys., B10, 191 (1974).

[10] Wu J.B.C, Li J.C.M., J. Mater. Sci.,434 (1976).

[11] Donald A.M., Kramer E.J., J. Mater. Sci., 16, 669 (1981).

[12] Donald A.M., Kramer E.J., J. Mater. Sci., 16, 2977 (1981).

[13] Argon A.S., Hannoosh J.G., Phil. Mag., 36, 1195 (1977).

[14] Taylor G.I., Proc. Roy. Soc. A 201, 192 (1950).

[15] Morgan G.P., Ward I.M., Polymer 18, 87 (1977).

[16] Kramer E.J. and Berger L.L., Adv. Polym. Sci. 91/92 (1990).

[17] Donald A.M., Kramer E.J. and Bubeck, R.A., J. Polym. Sci. Polym. Phys. Ed., 20, 1129 (1982).

[18] Donald A.M., Kramer, E.J, J. Polym. Sci. Polym. Phys. Ed., 20, 899 (1982).

[19] Donald A.M., Kramer, E.J., Polymer, 23, 461 (1982).

[20] Donald A.M., Kramer, E.J., Polymer, 23, 1183 (1982).

[21] Henkee C. S., Kramer E. J., J. Polym. Sci. Phys. Ed., 22, 721 (1984).

[22] Fetters L.J., Lohse D.J., Richter D, Witten T.A., Zirkel A., Macromolecules, 27, 4639 (1994).

[23] Fetters L. J., Lohse D. J., Graessley W. W., J. Polym. Sci., Part B: Polym. Phys. 37, 1023 (1999).

[24] Brown H.R., Russell T.P., Macromolecules, 29, 798 (1996).

[25] Brown H.R., Macromolecules, 34, 3720 (2001).

[26] Oslanec R., Brown H.R., Macromolecules, 36, 5839 (2003).

[27] Silberberg A.J., Colloid Interface Sci. 90, 86 (1982).

[28] Ganesan V, Pryamitsyn V., Macromolecules, 35, 9219 (2002).

[29] Jones R. A. L and Richards R. W., *Polymers at Surfaces and Interfaces*, Cambridge University Press, (1999).

[30] Forrest J.A., Dalnoki-Veress K, Adv. Colloid Interf. Sci. 94, 167 (2001).

[31] de Gennes P-G, *Scaling Concepts in Polymer Physics*, Cornell University Press: Ithaca and London, (fifth printing) (1996).